FEASIBILITY STUDY
FOR RERIGGING THE HAYSTACK ANTENNA

M. S. Zarghamee

H. Simpson

Prepared by

SIMPSON GUMPERTZ & HEGER INC.

For

MASSACHUSETTS INSTITUTE OF TECHNOLOGY
LINCOLN LABORATORY

23 FEBRUARY 1967

FEASIBILITY STUDY
FOR RERIGGING THE HAYSTACK ANTENNA

M. S. Zarghamee

H. Simpson

REPORT NO. SGH-668-1

23 FEBRUARY 1967

Final Report

Prepared by

SIMPSON GUMPERTZ & HEGER INC.

For

MASSACHUSETTS INSTITUTE OF TECHNOLOGY
LINCOLN LABORATORY

Under

ABSTRACT

For the purpose of investigating the technical feasibility of rerigging the Haystack reflector, the following theoretical tools were developed:

1. A scheme was developed for the selection of an optimal sample of targets for predicting the error in the rms determination as affected by the size of sample.

2. Computer programs were written for processing and analysis of the optical surveys.

3. A statistical theory was derived for the prediction of surface deviations due to the random errors in the manufacture and rigging of the antenna.

4. A computer program was developed for the calculation of the radiation pattern of the reflector from the known surface errors.

5. An extension of Ruze's theory was developed for the prediction of the gain loss and scatter of reflectors with nonuniform error distributions.

The results of one night survey and one day survey were analyzed; the calculated rms was 37 mils and 41 mils, respectively. The larger surface errors occurred in the inner panel region.

The gain and the half-power beamwidths corresponding to the measured surface deviations were calculated; good correlation with radiometric measurements was obtained.

Based on a detailed analysis of the rerigged reflector, on the assumption that only the inner panels are rerigged, the rms under average thermal conditions is predicted not to exceed 25 mils. Some further improvement can be achieved if cable forces and their pick-up angles are optimized.

PREFACE

ACKNOWLEDGMENT

TABLE OF CONTENTS

Table of Contents (continued)

TABLE OF FIGURES

Number

Table of Figures (Continued)

1. INTRODUCTION

1.1   Purpose and Scope

This document is the final report of the work performed under Massachusetts Institute of Technology Lincoln Laboratory Purchase Order C-444.

The purpose of the investigation reported herein is to predict, from mathematical analyses based on optical survey data, the extent of improvement that can be achieved in the Haystack antenna by an appropriate rerigging of the reflector.

The scope of the investigation is as follows:

1.   To develop software for the analysis of zenith-position optical surveys, and for obtaining the root mean squares and contour maps of effective surface deviations of the reflector for selected elevation angles.

2.   To evaluate the accuracy of the analyses by comparison with radiometric measurements.

3.   To predict the properties of the rerigged reflector by selecting an appropriate region for rerigging and calculating the deterministic surface deviations as well as the effects of the random errors which will be introduced in the rerigging process.

Chapter 2 of this report describes a theory for the selection of a sample of targets for the optical survey and a discussion of the effects of this sampling on the estimates of the reflector characteristics. A description of the method of analysis of survey measurements and the results obtained are given in Chapter 3. Comparison with radiometric measurements are presented and discussed in Chapter 4.   Chapter 5 contains the development of the methods for the deterministic and stochastic prediction of the behavior of the rerigged antenna. A summary of the results obtained and conclusions are given in Chapter 6.

1.2   Description of Reflector Surface

The paraboloidal surface of the Haystack antenna is composed of an inner row of 32 panels and an outer row of 64 panels. A one-inch thick splice plate composed of 32 segments joins the inner and the outer panels. The panels are supported on a system of standoff studs that are normal to the surface, and two lines of shear studs oriented parallel to the RF axis. Expanders are provided at all radial joints for rigging purposes. These expanders are designed to act also as shear keys between the adjacent panels. On the back surface of the reflector there is a system of circumferential, preloaded cables guided on rollers. The rollers located near the panel edges are mounted close to the back surface. For rigging purposes, the rollers in the middle of panels can be displaced from the back surface, thus permitting variation of the force applied normal to the panel surface.

On the surface of the reflector, there is a set of primary targets (rows A through H) and a set of secondary targets (rows J through P). There are 64 targets on each of the target lines A, J, B, K, C, L, and D, and 128 targets on each of the target lines M, E, N, F, O, G, P, and H, totalling 1472 targets in all. The target locations were established on the panels by reference to a system of tooling holes. The original rigging of the reflector surface was achieved by bringing each target to within a specified allowable tolerance of its theoretical location, as specified in the bias rigging table.

1.3   Historical Background

Following the original rigging of the Haystack reflector, a series of calibration measurements by D. G. Stuart, made for the purpose of developing a calibration chart for the optical probe, indicated that the probe contained serious errors. These errors, which were as high as 43 seconds of arc, were found to be caused by corrosion of the mirror positioning button [1]. Following this discovery, a committee was formed to study the feasibility of rerigging the reflector. In its final report [2], the Committee recommended that the Haystack antenna be rerigged by the theodolite-tape method; the implication was that direct optical and tape measurements should be made from the RF axis to each rigged point.

2

An alternate method of rerigging, based on the use of the distances between targets located on the same radial line and of a theodolite for optical measurements, was analyzed by M. S. Zarghamee and H. Simpson [3,4]. The method consists of locating the splice plate targets by tape-and-theodolite and then proceeding to locate the other targets by the use of the theodolite alone. This method assumes that an error bound can be established for the distances between targets. It was concluded from this investigation that, if the effects of thermal distortions can be neglected, the targets can be rigged to within approximately 7 mils rms.

The thermal distortions were first observed by North American Aviation [5] during the initial rigging process. Measurements indicated that targets on the Haystack reflector undergo large movements over periods of several hours. A subsequent investigation performed by Dynatech [6] revealed that the differences in the thermal time constants of the various structural components of the antenna when subjected to diurnal ambient termperature excursions cause large transient differences in the temperatures of various groups of members. (A maximum temperature difference of 10°F was predicted between the splice plate and the panels of the reflector.) A thermal analysis of the antenna in the face-up attitude was performed by Simpson Gumpertz & Heger Inc. [7], employing the results of the Dynatech investigation. It was concluded that the thermal lag of the splice plate is the major source of thermally induced distortions; the magnitude of these distortions overshadows those caused by the temperature differences in the other structural components. It was recommended that corrective measures be taken to remedy this problem. To reduce the time constant of the splice plate, it was decided to paint it black. Subsequent measurements showed a maximum observed temperature difference between splice plate and panels of less than 3 degrees. This reduces the calculated maximum thermally induced distortion, assuming an axisymmetric temperature distribution, from 35 mils rms to 10 mils rms.

2.   TARGET SAMPLING

2.1   Introduction

The original rigging of the Haystack reflector was performed in the face-up position by bringing the primary and secondary targets to within specified tolerances of the biased surface. (The biased surface of the antenna in the face-up position was taken as the surface which deviates from the perfect paraboloidal surface by one-half the maximum difference encountered in the static dead weight deflection of the antenna in tilting from face-up to face-side attitude.) To obtain an idea of the surface deviations in the present dish and to predict the level of improvement that can be achieved, a survey of the reflector was necessary. Obviously, it was desirable to include as many targets as practicable in the survey.

Since the surface deviations change noticeably with time [7], it was necessary to restrict the total time of the survey. Approximately stable thermal conditions have been observed for a period of a few hours starting about midnight. This established an approximate upper limit for the total number of targets that could be included in the survey. This limit corresponded to approximately one-third of the total number of targets.

The problem of selecting an optimum distribution of targets as well as the effects of the total number of targets selected on the accuracy of the results obtained are discussed in this chapter. The problem is formulated as one of stratified random sampling, with inboard and outboard targets each forming a sampling stratum. The optimal distribution is determined and the effect of the size of the sample space on the variance of the predicted rms is studied.

2.2   Theory of Stratified Random Sampling

In random sampling from a population, the size of the sample as well as the technique of sample selection affect the efficiency of the sampling investigation. The process of

4

dividing the population into parts prior to sampling and then drawing random samples from each part separately is called stratified random sampling. For maximum efficiency of the estimation, the distribution of the sample population among the various parts must be determined in an appropriate manner.

Consider the total target population of size N subdivided into k strata. Denote the size of the jth stratum by N_j. For the ith target in the jth stratum, define x_{ij} as follows:

$$x_{ij} = N \frac{A_{ij} F_{ij} \epsilon_{ij}^2}{\Sigma A_{ij} \cdot F_{ij}} \tag{2.1}$$

where
A_{ij} = the area associated with the target,

F_{ij} = the illumination factor associated with the target,

ϵ_{ij} = the effective surface deviation of the target from the best-fit paraboloid,

and the denominator is the sum of all the products of the area and illumination factors.

The mean of all the x_{ij}'s is equal to the square of the root-mean-square of the effective surface deviation of the antenna weighted by the area and illumination factors; that is

$$\bar{x} = \frac{1}{N} \sum x_{ij} = \frac{\Sigma A_{ij} F_{ij} \epsilon_{ij}^2}{\Sigma A_{ij} F_{ij}} = (rms)^2 \tag{2.2}$$

Let x_j be the mean and σ_j^2 be the variance of the x_{ij}'s in the jth stratum; therefore,

$$x_j = \frac{1}{N_j} \sum_{i=1}^{N_j} x_{ij} \tag{2.3}$$

and
$$\sigma_j^2 = \frac{1}{N_j} \sum_{i=1}^{N_j} (x_{ij} - x_j)^2 \tag{2.4}$$

5

The mean of all the x_{ij}'s may then be defined as follows:

$$\bar{x} = \frac{1}{N} \sum_{j=1}^{k} N_j x_j \qquad (2.5)$$

Assume that we want to take a sample of total size n; the population of the sample space in the jth stratum is designated by n_j. To predict the rms of the dish, we first estimate x_j in each stratum and then employ Eq. (2.5) to estimate the value of $\bar{x}$. If we denote the estimated value of x_j by

$$z_j = \frac{1}{n_j} \sum_{i=1}^{n_j} x_{ij} \qquad (2.6)$$

the variance of this estimator (this variance is a measure of the accuracy of the sampling only) in the jth stratum is given as follows:

$$\sigma^2_{z_j} = \frac{N_j - n_j}{N_j - 1} \frac{\sigma_j^2}{n_j} \qquad (2.7)$$

where $\sigma^2_{z_j}$ is the variance of the estimator in the jth stratum if sampling is performed without replacement [8]. It is of interest to note that when $n_j = N_j$, that is when all the targets in the jth stratum have been selected in the sample space, then the variance of the estimator in that stratum vanishes; on the other hand, for a sample space of only one target, the variance of the estimator is equal to the variance of the x_{ij}'s in that stratum.

The variance of the estimator for the total target space is then given by the following equation:

$$\sigma^2_z = \sum_{j=1}^{k} \frac{N_j^2}{N^2} \sigma^2_{z_j} = \sum_{j=1}^{k} \left(\frac{N_j - n_j}{N_j - 1} \frac{\sigma_j^2}{n_j} \right) \frac{N_j^2}{N^2} \qquad (2.8)$$

To optimize the choice of samples, the value of the number, n_j, of sample targets in each stratum is chosen to minimize the variance of the estimator. To perform this optimization,

we let the partial derivative of σ_z^2 with respect to the number of targets in each stratum vanish, subject to the condition that the total number of targets remains constant, that is

$$\sum_{j=1}^{k} n_j = n \tag{2.9}$$

Let us then write Eq. (2.8) in the following form:

$$\sigma_z^2 = \frac{1}{N^2} \left[\sum_{j=1}^{k-1} \frac{N_j^3 \sigma_j^2}{(N_j-1)n_j} + \frac{N_k^3 \sigma_k^2}{(N_k-1)n_k} \right] - \frac{1}{N^2} \sum_{j=1}^{k} \frac{N_j^2 \sigma_j^2}{N_j - 1} \tag{2.10}$$

If we express n_k in terms of $n_1, n_2, \ldots, n_{k-1}, n$ and perform the differentiation, we obtain

$$\frac{\partial \sigma_z^2}{\partial n_j} = -\frac{N_j^3 \sigma_j^2}{N^2(N_j-1)n_j^2} + \frac{N_k^3 \sigma_k^2}{N^2(N_k-1)n_k^2} = 0 \quad \text{for } j = 1,2,\ldots,k-1 \tag{2.11}$$

The above equation implies that

$$\frac{N_j^3 \sigma_j^2}{N^2(N_j-1)n_j^2} = \text{constant} = Q^2 \tag{2.12}$$

For N_j much larger than unity, we can write

$$n_j = \frac{N_j \sigma_j}{N Q} \tag{2.13}$$

Noting that $n = \sum_{j=1}^{k} n_j$, then the value of Q may be obtained as follows:

$$n = \sum_{j=1}^{k} \frac{N_j \sigma_j}{NQ} \tag{2.14}$$

or

$$Q = \frac{1}{Nn} \sum_{j=1}^{k} N_j \sigma_j \tag{2.15}$$

Substituting Eq. (2.15) into Eq. (2.13), we get

$$n_J \text{ (optimum)} = n \frac{N_J \sigma_J}{\sum\limits_{i=1}^{k} N_i \sigma_i} \tag{2.16}$$

and

$$\sigma_z^2 = \frac{1}{nN^2} \left[\sum\limits_{J=1}^{k} N_J \sigma_J \right]^2 - \frac{1}{N^2} \sum\limits_{J=1}^{k} N_J \sigma_J^2 \tag{2.17}$$

If there is only one stratum, we obtain from Eq. (2.17)

$$\sigma_z^2 = \frac{\sigma^2}{n} - \frac{\sigma^2}{N} \tag{2.18}$$

and the error reduces to zero as n approaches N.

Note that Eq. (2.18) and Eq. (2.17) have the same form, differing only in the coefficients of the variance function.

2.3 Application to Haystack Antenna

The analysis of an optical survey of the Haystack reflector [9] revealed that there are highly variable surface deviations in the inner 30-foot radius of the aperture; the errors in the outer 30 feet are significantly less. Therefore, it is reasonable to assume two sampling strata, one consisting of all the targets on the inboard panels and another stratum consisting of all the targets on the outboard panels. An estimate of the values of the variance of x_{iJ} (x_{iJ} defined by (Eq. 2.1)) was obtained from the analysis of this survey. It was found that

$$\sigma_1 = .00339$$

and

$$\sigma_2 = .00088.$$

From Eq. (2.16), the ratio of the number of selected targets in the inboard panels to those located on the outboard panels is about 1.35 for optimal sampling technique. Using Eq. (2.17), the variance of the sampling may then be expressed as follows:

$$\sigma_z^2 = \frac{2.325 \times 10^{-6}}{n} - 2.43 \times 10^{-9}$$

It is emphasized that this equation gives the variance of the square of the predicted rms of the surface. The plot of the standard deviation of the predicted $(rms)^2$ with the number of targets in the sample space is given in Fig. 1. This figure indicates that the standard deviation of the predicted rms of the reflector, assuming that its actual value is about .04 inches, is approximately .0005 inches for about 600 targets, .001 inches for about 270 targets, and .002 inches for about 100 targets.

Optimal sampling schemes adopted for 424- and 212-target sample spaces are shown in Figs. 2 and 3, respectively. Assuming again that the actual rms is about .04 inches, the expected standard deviation of the estimated rms will be about 1.3 percent for the 424-point sample and about 2.7 percent for the 212-point sample. In both sampling schemes, the total number of targets in each sampling stratum is divided uniformly amongst the edge targets, center targets, and different target rows.

A 424-point survey was made in the early hours of the morning of 1 September 1966 by D. G. Stuart and C. T. Frericks. The duration of the survey is estimated at less than three hours. A 212-point survey was made after 1 p.m. on 30 August 1966. This survey took about one hour. The weather was cloudy and the temperature was about $88^\circ F$. The splice plate in both cases was painted black.

3.   ANALYSIS OF OPTICAL SURVEYS

3.1   Introduction

The analysis of an optical survey consists of the prediction of the reflector tolerances through analysis of a set of optical measurements to the selected sample of targets. An important assumption in this analysis is that the deflections at the target points are in fact representative of the deflections between targets. This assumption seems reasonably valid from the manner in which the panels are supported in reference to the location of the target points. An indication of the accuracy of this assumption can be obtained by comparing the results of this investigation to those of the radiometric measurements.

Each optical survey consists of a set of zenith angles measured from the reference axis of the theodolite, located on or very near the RF axis, to the lines of sight to the selected targets. The exact location of theodolite and the angular orientation of its reference axis with respect to the RF axis are not known.

To define the reflector surface, a distance parameter is also required. This is obtained by establishing error bounds for the theoretical distances between targets and from radial measurements to the splice plate targets.

The radii to the splice plate targets were measured during the original rigging process from a point on the vertical reference axis of the antenna structure. Since during the optical survey radial distance measurements were not taken to the splice plate targets, the original radial measurements are adopted for this analysis. Furthermore, it is assumed that these measurements are in fact taken from the actual RF axis, that is, the axis of the best-fit paraboloid. The effect of this assumption is discussed later in this chapter.

The surface deviations from the best-fit paraboloid cause changes in the path lengths of the RF waves, which may result in phase errors and hence loss of gain. It can be shown [3] that the RF direction (z) component of the normal surface displacement at any point

is equal to one-half the change in the RF path length of the reflected waves at that point. This distance is referred to as the effective surface deviation (after J. Ruze).

A measure of surface accuracy useful for predicting RF performance is the rms of the reflector, which is defined here as the square root of the mean of the weighted squares of the effective surface deviation. The weighting function is the illumination distribution over the aperture. This rms is expressed as follows:

$$\text{rms of the reflector} = \left[\frac{\int_A f(\bar{r})\ \epsilon^2(\bar{r})\ dS}{\int_A f(\bar{r})\ dS} \right]^{\frac{1}{2}} \tag{3.1}$$

where

$\bar{r}$ = aperture position vector,

$\epsilon(\bar{r})$ = effective surface deviation at the point defined by $\bar{r}$,

$f(\bar{r})$ = the illumination function at the point defined by $\bar{r}$, and

A = the aperture area.

In this chapter the illumination function is assumed to have a paraboloid-on-a-pedestal distribution with a 12 db edge taper (Fig. 18).

The method of analysis and the results obtained are discussed in the following sections.

3.2   Method of Analysis

Employing the zenith-angle measurements, the effective surface deviations with respect to the best-fit paraboloid may be calculated for any desired position of the antenna as follows:

1.   Assume an initial reference paraboloid with the same focal length as the theoretical design paraboloid and located near the estimated position of the best-fit paraboloid.

2.   Compute at each measured target the effective surface deviations with respect to the initial reference paraboloid.

11

3.   Determine the best-fit paraboloid by minimizing the rms of the effective surface deviations with respect to the rigid body movements and change in the focal length of the initial reference paraboloid.

4.   Compute the effective surface deviations with respect to the best-fit paraboloid, and the rms of the reflector.

5.   Add to the best-fit surface deviations the dead weight travels of the surface points in going from zero to any desired zenith angle and repeat the best-fitting process.

The initial reference paraboloid may be assumed to be oriented so that its axis coincides with the vertical axis of the theodolite. The elevation of its apex below the theodolite may be taken as the average height of instrument calculated from the measured zenith angles of a small set of targets by assuming temporarily that these targets are at their theoretical design locations. The initial reference paraboloid thus obtained will not be far from the best-fit paraboloid. Therefore, the rigid body movements and the change in the focal length of the initial reference paraboloid will be small enough to permit appropriate linearization.

The general theoretical development pertaining to the method is presented in Section 3.3; Sections 3.4, 3.5, and 3.6 are devoted to detailed descriptions of the computational procedure.

3.3   Theoretical Development

The location of the best-fit paraboloid may be expressed in terms of the location of the initial reference paraboloid by a vector U whose six components are as follows:

u_1 , u_2 , u_3 =   the x-, y-, and z-components of the distance vector between points T and T' located on the reference axes of the initial and the best-fit reference paraboloid, respectively (Figs. 5 and 6),

u_4, u_5 = the x- and y-components of the vector defining the rotation of the axis of the best-fit paraboloid with respect to the axis of the initial reference paraboloid, and

u_6 = the difference in the focal lengths of the best-fit paraboloid and the initial reference paraboloid.

At a point on the aperture defined by the position vector $\bar{r}$, the effective surface deviation $\epsilon(\bar{r})$ after a small shift of the reference paraboloid may be calculated as follows:

$$\epsilon(\bar{r}) = \epsilon_o(\bar{r}) + \sum_{i=1}^{6} u_i \, \epsilon_i(\bar{r}) \qquad (3.2)$$

where $\epsilon_o(\bar{r})$ = the effective surface deviation at this point with respect to the initial reference paraboloid, and

$\epsilon_i(\bar{r})$ = the effective surface deviation at this point due to a unit u_i.

We now seek those values of u_i for $i = 1, 2, \ldots, 6$ which minimize the rms of the effective surface deviation; that is,

$$\frac{\partial (\text{rms})}{\partial u_i} = 0 \qquad \text{for } i = 1, 2, \ldots, 6 \qquad (3.3)$$

It can be easily shown that the above requirement is equivalent to the following:

$$\int_A \epsilon(\bar{r}) \, \epsilon_i(\bar{r}) \, f(\bar{r}) \, dS = 0 \qquad i = 1, 2, \ldots, 6 \qquad (3.4)$$

If Eq. (3.2) is substituted in the above equation, a system of six equations is obtained, in terms of the six u components, as follows:

$$[B] \, \{U\} = \{C\} \qquad (3.5)$$

where the terms of the matrices B and C are given by

$$b_{ij} = \int_A \epsilon_i(\bar{r}) \, \epsilon_j(\bar{r}) \, f(\bar{r}) \, dS \qquad (3.6)$$

and $\quad c_i = -\int_A \epsilon_i(\bar{r}) \, \epsilon_o(\bar{r}) \, f(\bar{r}) \, dS \qquad (3.7)$

13

If ϵ_o, ϵ_1, ..., ϵ_6 are known the components of the U vector may be calculated from Eq. (3.5), and Eq. (3.2) and Eq. (3.1) may be employed to calculate the rms of the reflector.

3.4 Calculation of Surface Deviations from Initial Reference Paraboloid

The method of calculation of the surface deviations from the initial reference paraboloid consists of computing the surface deviations at the splice plate targets and then moving outboard and inboard from the splice plate to locate each successive row of targets. The splice plate targets can be located by a theodolite and radial distances from a known point.

In the present investigation, it is assumed that the radial measurements to the splice plate targets by North American Aviation during the initial rigging process were made from the axis of the best-fit paraboloid. (Error sensitivity due to this assumption was checked by computing the effective surface deviations due to an arbitrary displacement of this reference point; the calculated rms of the effective surface deviations thus obtained was less than 4.5 percent of the magnitude of the displacement of the reference point.) Since the actual location of the best-fit paraboloid is not known a priori, the radial measurements are first considered to be with respect to the axis of the initial reference paraboloid. Due to the rigid body movements of the initial reference paraboloid, changes are introduced in these radial distances. These changes are corrected (see Section 3.5) so that the radial distances of the splice plate targets from the axis of the shifted paraboloid are identical to the values measured by North American Aviation.

Once the splice plate targets have been located, the locations of the successive outboard and inboard targets can be obtained from the angular measurements and the known distances between targets.

Since small quantities are to be determined from combinations of large numbers, the arithmetic computation is susceptible to large round-off errors. This problem can be overcome

by working with the deviations of the angular measurements from the theoretical design values obtained for the initial reference paraboloid.

The effective surface deviation obtained from the intersection of the line of sight from point P on the axis of the initial reference paraboloid (Fig. 4) and a distance d from a known point Q is given by the following equation (for derivation see Section 5.3):

$$\epsilon = \frac{1}{\left[1 + \left(\frac{r}{2f}\right)^2\right](\cot \psi_o + \cot \alpha)} \left[\delta \csc \alpha \left(\cot \psi_o - \frac{r}{2f}\right) + \omega \csc^2 \psi_o (\cot \alpha \, r + 2z)\right] \quad (3.8)$$

where ω = the angular error in the line of sight; positive as shown in Fig. 4

δ = the error in the distance QR

In these equations the angular and distance errors are assumed to be small when compared to the dimensions of the antenna. This in fact is the case, since we have purposely selected the initial reference paraboloid very close to the best-fit paraboloid. The errors in the origins of the points P and Q may be converted to equivalent δ and ω errors. The detailed explanation of this conversion is presented in Reference 3.

In the application of the above procedure, the known (deterministic) distance errors between targets on the same panel as well as the known distance errors between the splice plate targets and the first targets on the adjacent panels are included. For errors which are random in nature, the analysis method of Chapter 5 may be employed. However, the results of an investigation of the effects on the rms of the reflector of the estimated random errors in the distances between targets on the same panel and in the connection between the splice plate and panels revealed that these errors are small and that their effects on the rms of the reflector can be considered negligible.

3.5   Effect of Movements of Initial Reference Paraboloid

In the following paragraphs   the effects of unit rigid body translations, unit rigid body rotations, and a unit change of the focal length of the initial reference paraboloid upon

15

the effective surface deviation at a target are formulated.

The effective surface deviation, ϵ, was indicated in Section 3.1 to be the z-component of the normal error. If $\hat{n} = (n_x, n_y, n_z)$ denotes the unit normal vector to the reflector surface at a point on the reflector and $\overline{w} = (u, v, w)$ is the displacement vector at that point, then

$$\epsilon = n_z \, (\hat{n} \cdot \overline{w}) . \tag{3.9}$$

3.5.1 Effect of a Unit x-Displacement.

Consider a unit x-displacement of the initial reference paraboloid (Fig. 5). As a result of this rigid body translation, the radial distance of the splice plate targets will differ from that measured with respect to the initial reference paraboloid by $-\cos \varphi'$ (φ' as defined in Fig. 17). Then

$$\epsilon_1 = n_x n_z - \epsilon_{sp} \cos \varphi' \tag{3.10}$$

where ϵ_{sp} is the effective surface deviation due to a unit increase in the radial distance of the splice plate targets. The value of ϵ_{sp} may be calculated from Eq. (3.8).

The effect of a unit y-displacement may similarly be calculated.

3.5.2 Effect of a Unit z-Displacement.

Consider a unit z-displacement of the initial reference paraboloid (Fig. 6). Since such a rigid body displacement does not change the radial distance of the splice plate targets, then

$$\epsilon_3 = n_z^2 \tag{3.11}$$

3.5.3 Effect of a Unit x-Rotation.

Consider a unit rigid body rotation of the initial reference paraboloid about an axis through the theodolite and parallel to the x-axis (Fig. 7). This rigid body rotation causes a change in the radial distance of the splice plate targets

equal to $(z_{sp} - z_t) \sin \varphi'$, where z_t is the height of instrument and z_{sp} is the z-coordinate of the splice plate. Then

$$\epsilon_4 = (z_{sp} - z_t) \sin \varphi' \, \epsilon_{sp} + n_z \cdot (n_y(z_t - z) + n_z y) \qquad (3.12)$$

The effect of a unit y-rotation may similarly be formulated.

3.5.4 Change in the Focal Length.

A change in the focal length of the initial reference paraboloid produces a surface deviation in the direction of the RF axis. This deviation is given by the following equation:

$$\Delta z = \frac{\partial}{\partial f} \left(\frac{r^2}{4f} \right) \Delta f$$

or

$$\Delta z = - z \left(\frac{\Delta f}{f} \right)$$

Hence, the effective surface deviation for a unit change in the ratio $(\Delta f/f)$ would be

$$\epsilon_6 = - (n_z)^2 z \qquad (3.13)$$

3.6 Effects of Dead Weight Travels

The surface deviations calculated with respect to the best-fit paraboloid in the face-up position may be modified by the effects of the shift in the gravity vector as the antenna tilts from zero to any desired zenith angle, thus yielding the surface deviations of the antenna in that position. The travel of a point as the antenna moves from face-up to zenith angle φ is obtained by the following equation:

$$\bar{w}(\alpha) = \bar{w}_u (\cos \alpha - 1) + \bar{w}_s \sin \alpha - \bar{w}_{c_2} \langle \cos \alpha \tan \beta \rangle \qquad (3.14)$$

where $\bar{w}$ = dead weight travel of a point from face-up position to zenith angle α,

$\bar{w}_u$ = dead weight deflection of the point in the face-up position,

17

$\bar{w}_s$ = dead weight deflection of the point in the face-side position,

$\bar{w}_{c_2}$ = dead weight deflection of the point due to the action of the center cable in the face-side attitude,

β = zenith angle at which center cables start to pick up load, and

$\langle g \rangle$ = 0 for $\alpha - \beta < 0$

= g for $\alpha - \beta \geq 0$.

The values of $\bar{w}_u$, $\bar{w}_s$, and $\bar{w}_{c_2}$ are obtained from a previously performed static analysis of the antenna by the FRAN computer program. (Note that these values do not include the effects of the weight of the net that has recently been attached to the antenna.) From these, the best-fit reference paraboloid through the modified surface deviations is obtained and the effective surface deviation with respect to this paraboloid and the rms of the reflector are calculated.

3.7   Results and Conclusions

The rms of the reflector (the root mean of the illumination-weighted square of the effective surface deviation from the best-fit paraboloid – Eq. (3.1)) was computed for elevation angles between zero and 90 degrees, employing the 424-point night survey results. The variation of the rms over the elevation coverage is indicated in Fig. 8. The calculated rms of the reflector in face-up position is 0.036 inches. As the zenith angle increases, the rms of the reflector increases until it reaches .037 inches, at which point the center cable starts to pick up load. The rms of the reflector then decreases to a minimum of .034 inches in the vicinity of 75 degrees zenith angle before starting to rise again.

The rms of the reflector in the face-up attitude calculated from the daytime measurements is about .041 inches.

Contour maps of the effective surface deviations of the reflector, based on the night survey, are shown for different elevation angles in Figs. 9 through 15. Fig. 16 is a contour map of the effective surface deviations of the reflector in the face-up attitude for the day survey.

18

Analyses of the distribution of the surface deviations, which may be observed only partially from the contour maps, revealed that

1.   For the night survey, the larger surface deviations are located in the region of the inner panels; the outer panels indicate significantly less distortion. (For the inboard and outboard targets , the rms of their effective surface deviations from their own best-fit paraboloid was calculated separately. The results indicated that the rms of the inboard targets is approximately twice that of the outboard targets.)

2.   The day survey gave a distribution of surface deviations very similar to that of the night survey; the observed increases in magnitude occurred primarily in the inner panel region.

3.   For both the day and the night surveys, the distribution of the error in the region of the inner panels did not change significantly with the zenith angle of antenna.

4. EXPERIMENTAL VERIFICATION

4.1 Introduction

To test the validity of the analysis performed in the last chapter, gain and half-power beamwidth will now be calculated and compared with the results of the radiometric measurements.

4.2 Computation of Gain and Radiation Pattern

The axial gain of the existing reflector and its radiation pattern may be computed from the surface deviations obtained from the analysis of the optical survey by the following equation:

$$G(\theta,\varphi) = \frac{4\pi}{\lambda^2} \frac{\left| \int_A f(\bar{r}) \, e^{j\bar{k}\cdot\bar{r}} \, e^{j\delta(\bar{r})} \, dS \right|^2}{\int_A f^2(\bar{r}) \, dS} \tag{4.1}$$

where

λ = the wavelength,

$f(\bar{r})$ = the illumination function at point $\bar{r}$ of the aperture,

$\delta(\bar{r})$ = $\dfrac{4\pi\epsilon(\bar{r})}{\lambda}$ = the phase error or aberration function at point $\bar{r}$ of the aperture,

$\bar{r}$ = the aperture position vector,

$\bar{k}$ = $\dfrac{2\pi}{\lambda}\bar{p}_o$ where $\bar{p}_o$ is a unit vector in the direction of observation,

(θ,φ) = angles defining the direction of observation (see Fig.17),and

A = the area of the aperture.

A program was written to evaluate the above integral for given values of ϵ and for a range of values of φ and θ, thus establishing the radiation diagram of the antenna. For the face-up attitude, the radiation pattern is shown in Figs. 19 and 20 for the 424-point night

survey and in Figs. 21 and 22 for the 212-point day survey. The results are shown for 15.75 GHz (λ = 1.94) and 8.25 GHz (λ = 3.64) and a parabola-on-a-pedestal illumination function with 12 db edge taper.

In the following table are listed some of the pertinent results obtained:

	Night Survey	Day Survey
RMS	0.0366 inches	0.0413 inches
Axial Gain		
15.75 GHz	73.37 decibels	72.75 decibels
8.25 GHz	68.96 decibels	68.68 decibels
Half-Power Beamwidth		
15.75 GHz	33.0 millidegrees	32.35 millidegrees
8.25 GHz	63.5 millidegrees	62.8 millidegrees

Note that the axial gain at the higher frequency exceeds that at the lower frequency by about 4.4 db for the night survey and about 4.1 db for the day survey.

4.3   Experimental Results

The flux of Cas A, a radio source within constellation Cassiopeia, was measured on the cornucopia by Mr. R. J. Allen. After reduction to a similar feed basis and applying corrections for waveguide and rotary joint effects, the following results were obtained [11]:

Date	Frequency	Feed	Efficiency at Feed Flange	HPBW
Mar. 1966	15.75 GHz	Horn	24.0 %	35.8 md
Dec. 1965	8.25 GHz	Clavin	40.9 %	70.8 md

The gain of the antenna may be expressed as follows:

$$G = \eta \frac{4\pi A}{\lambda^2} \tag{4.2}$$

Hence

$$\frac{G_1}{G_2} = \frac{\eta_1}{\eta_2} \left(\frac{\lambda_2}{\lambda_1}\right)^2$$

or

$$10 \log G_1 - 10 \log G_2 = 10 \log \left(\frac{\eta_1}{\eta_2}\right) + 20 \log \left(\frac{\lambda_2}{\lambda_1}\right)^2 \tag{4.3}$$

which represents the difference, in db, between the gains at the two wavelengths.

Substituting into Eq. (4.3) the experimental results tabulated above, we find that an increase in frequency from 8.25 GHz to 15.75 GHz is associated with an increase in gain of 3.3 db.

The 3.3 db increase includes the effect of radome losses, which have been calculated by J. Ruze to be 1.2 db and 1.7 db at 8.25 GHz and 15.75 GHz, respectively. This represents a decrease in gain of 0.5 db at the higher frequency. These loss calculations, however, assumed a 0.032 inch thick radome membrane. According to Mr. E. Murphy of Lincoln Laboratory, the actual thickness is probably somewhat larger than this figure. Furthermore, the radome has two layers of paint. These effects are completely negligible at 8.25 GHz but are significant at 15.75 GHz. Accordingly, the decrease in gain due to radome losses is estimated to be at least 0.7 db. Since the radome measured increase in gain at the higher frequency is 3.3 db, the measured increase associated with the antenna itself is at least 4.0 db.

4.4   Correlation of Results of Optical Survey with Radiometric Measurements

The 4.0 db increase in gain at 15.75 GHz calculated in Section 4.3 from the radiometric measurements compares with the values 4.4 db and 4.1 db obtained in Section 4.2 from the analyses of the night optical survey and day optical survey, respectively. The agreement in the difference of axial gain is quite good. The explanation for the digit discrepancy may be in the differences in the thermal conditions of the antenna. The radiometric

22

measurements were made before the splice plate was painted black; also, the antenna was not in the face-up attitude, and hence the temperature distribution was not axisymmetric.

The half-power beamwidths calculated from the results of the optical surveys are somewhat smaller than those measured. Part of this discrepancy may be due to the nonuniformity of the radome blockage over the aperture. Since the members of the radome space frame have larger depths than widths, the blockage is minimum at the center of the aperture and is maximum at the outer edge. A blockage of .3 db at the center and 1.2 db at the edge of the reflector has been calculated by J. Ruze [13]. The effect of this blockage variation on the antenna gain and on the radiation pattern is similar to that resulting from an increase of 0.9 db in the taper of the illumination function.

Another reason for the discrepancy in half-power beamwidth is in the difference of the edge taper of the illumination pattern produced by the Clavin feed and that of the horn feed. The Clavin feed has an edge taper of 12 db, whereas the taper of the horn feed is about 14 db. Considering also the effect of the radome blockage, the effective edge taper at 15.75 GHz is about 15 db and that at 8.25 GHz is about 13 db. The adjusted half-power beamwidths are as follows:

	Night Survey	Day Survey
RMS	36.6 mils	41.3 mils
Half-power Beamwidth		
15.75 GHz (15 db edge taper)	33.9 md	33.1 md
8.25 GHz (13 db edge taper)	64.4 md	63.6 md

At least a part of the remaining discrepancy may be associated with the width of the radio source and with the scatter of the experimental results. Recent radiometric measurements by Dr. Meeks estimate the HPBW at about 36 md at 15.75 GHz and 69 md at 8.25 GHz for a point source. These values are respectively about 6 percent and 7 percent larger than the corresponding calculated values.

It is of considerable interest that the calculated results indicate a decrease in the half-power beamwidth with increasing rms. Significantly, this phenomenon was also observed by R. J. Allen through his radiometric measurements [12]. As it is shown in the theoretical development in Appendix A, this phenomenon is a characteristic of antennas with large errors near the center of their aperture.

The difference in the measured axial gain of the antenna between 8.25 GHz and 15.75 GHz may be employed to calculate the rms of the dish by means of Ruze's equation,

$$G_o = \eta \frac{4 \pi A}{\lambda^2} e^{-\left(\frac{4 \pi \epsilon}{\lambda}\right)^2} \tag{4.4}$$

Substituting in Eq. (4.4), the radiometrically measured difference of 4.0 db is found to correspond to an rms of reflector of about 41 mils. This is significantly less than the value of 54-55 mils rms that was formerly believed to be the surface accuracy. However, it compares favorably with the results of the optical survey, which are about 36.6 mils rms for the night survey and 41 mils rms for the day survey.

4.5   Conclusions

The results of this investigation indicate that the analyses of the optical surveys correlate reasonably well with the results of the radiometric measurements. Reasonable explanations have been found for the small discrepancies that exist. Therefore the analyses performed in Chapter 3, in which the surface deviation was obtained by analyzing only the deviations at the target points, appear to be valid.

The radiometric measurements indicate that an increase in the rms of the reflector corresponds to a decrease in the half-power beamwidth. This phenomenon was also observed through the analyses of the optical surveys. As is shown in Appendix A, this is a consequence of the fact that the larger errors are located near the center of the reflector. This observation confirms the conclusions reached in Chapter 3.

5. PROPERTIES OF THE RERIGGED REFLECTOR

5.1 Introduction

As was shown in Chapter 3, the present Haystack reflector has its largest surface deviations from the best-fit paraboloid in the region of the inner panels. It is important to know the level of improvement that can be achieved by rerigging only these panels. For the purposes of this investigation, it is assumed that the rerigging will result in zero nonrandom error at the rerigged targets when the antenna is in the 45-degree attitude. Therefore, for the rerigged reflector at any given position angle, the sources of surface deviations from a best-fit paraboloidal surface consist of the following:

a. the existing surface errors of the outer panels at the given elevation angle,

b. the dead load travels of the inner panels in going from 45 degrees to the given elevation angle, and

c. the random errors consisting of instrument errors, observer errors, manufacturing tolerances and rigging tolerances at the rerigged targets.

In this chapter, a stochastic method is presented for the determination of the effects of the random sources of error on the surface deviations and on the expected rms of the effective surface errors of the antenna. These errors are combined with the known deterministic errors and the expected rms of the rerigged dish is predicted.

It is important to note that in this chapter we have again assumed that the tolerance of the surface can be established through analysis of the surface deviations of the target points alone.

5.2 Nonrandom Surface Deviations of the Rerigged Reflector

Let us consider the nonrandom surface deviations of the rerigged reflector when the antenna is in the 45-degree attitude. The reference surface is obtained by passing a best-fit paraboloid through all the outboard targets and the targets located on the splice plate. The

inboard targets (the targets located on rows A,J,B,K,C, and L) are assumed to be rigged so that they have no nonrandom effective surface errors. (The amounts that the targets on the inner panels should be moved are their present deviations from this best-fit paraboloid when the antenna is tilted to 45 degrees.)

The rms of the nonrandom effective surface errors of the rerigged antenna is shown in Fig. 23 for the range of zenith angle coverage of the antenna. A contour plot of the deterministic effective surface errors of the rerigged antenna in the face-up position is shown in Fig. 24. This figure may be compared to Fig. 9, which shows the effective surface errors of the present dish.

5.3   Effects of Random Error

In this section a procedure is presented to calculate the statistical characteristics of the random surface deviations that will be produced at the rerigged targets. In brief, the procedure involves predicting the standard deviation and the frequency distribution function for each significant source of error involved in the rerigging of the inner panels. On the basis of these predicted values, the statistical properties of the distribution function of the effective surface error is obtained for the rerigged antenna. The following paragraphs contain the derivation of the governing equations and the application of these equations to the Haystack antenna.

5.3.1 Definition. For convenience, the error in rigging a target is divided into two parts, according to the source from which it originates. That portion of the error which is due only to the error in the line of sight and in the chord distance from the previously rigged point is designated "direct" error; the error resulting from the mislocation of the previously rigged points is designed "derived" error.

5.3.2 Derivation. A line of sight which passes through a known point P with coordinates $(0, z_o)$ and which makes an angle ψ with the vertical reference axis of the antenna intersects

a distance d from a known point Q at a point R (Fig. 4). The coordinates of point R may be established in terms of the coordinates of points P and Q, the angle ψ, and the distance d. If ψ and d are in error so that

$$\psi = \psi_o + \omega$$
$$d = d_o + \delta$$

(5.1)

where ψ_o and d_o are the expected (correct) values and ω and δ are the errors in ψ and d respectively, then the coordinates of the point of intersection may be obtained in terms of ω, δ, and the geometry of the system.

Since the errors ω and δ are small, a linearization of the errors in the coordinates of point R in terms of ω and δ may be performed; then:

$$\delta r = - \frac{\omega r \csc^2 \psi_o}{\cot \alpha + \cot \psi_o} + \frac{\delta \csc \alpha}{\cot \alpha + \cot \psi_o}$$

$$\delta z = + \frac{\omega r \csc^2 \psi_o \cot \alpha}{\cot \alpha + \cot \psi_o} + \frac{\delta \csc \alpha \cot \psi_o}{\cot \alpha + \cot \psi_o}$$

(5.2)

where δr and δz are the r- and z-components of the error at point R and α is defined in Fig. 4. The effective surface error is given by the following equation:

$$\epsilon = \frac{\delta z - \left(\frac{r}{2f}\right) \delta r}{1 + \left(\frac{r}{2f}\right)^2}$$

(5.3)

where f is the focal distance of the dish. If Eqs. (5.2) are substituted in this equation, after simplification we obtain

$$\epsilon = \frac{1}{\left[1 + \left(\frac{r}{2f}\right)^2\right]\left(\cot \psi_o + \cot \alpha\right)} \left[\delta \csc \alpha \left(\cot \psi_o - \frac{r}{2f}\right) + \omega \csc^2 \psi_o \left(\cot \alpha\, r + 2z\right)\right]. \quad (5.4)$$

28

The coefficients of δ and ω in Eq. (5.4) depend upon the geometry of the dish, the theoretical locations of the targets, and the location of the theodolite. If we denote these coefficients by a and b, then Eq. (5.4) may be written as follows:

$$\epsilon = a\delta + b\omega \qquad (5.5)$$

Let Δ and Ω be statistical variables corresponding to δ and ω respectively. The variable E denotes the effective surface error. Since

$$E = a\Delta + b\Omega \qquad (5.6)$$

the frequency distribution function, mean, and variance of E can be expressed in terms of frequency distribution functions, means, and variances of Δ and Ω.

If we assume that both Δ and Ω have normal Gaussian distributions with expected values of zero and standard deviations of σ_δ and σ_ω respectively, the effective surface error E would also have a normal Gaussian distribution with zero mean and a standard deviation σ_ϵ given by

$$\sigma_\epsilon = \sqrt{a^2 \sigma_\delta^2 + b^2 \sigma_\omega^2} \quad . \qquad (5.7)$$

If Δ and Ω have any distribution other than normal Gaussian, then Eq. (5.7) would still hold, but the probability of occurrence of σ_ϵ would depend upon the distribution function of E.

The effects of the derived errors and rigging tolerances may be now included by appropriate modification of the error in chord distance and error in the angle of theodolite.

Any error in the location of the previously rigged point, point Q, may be resolved into two components, parallel and normal to QR. The component of the error normal to QR will

29

not cause a significant error in the location of point R [3]. However, the component parallel to QR modifies the error in the distance d. In fact, the error in the distance d may be expressed by

$$\Delta = \Delta T + \Delta P + \Delta S \tag{5.8}$$

where ΔT = the error in chord distance between targets due target location error,

ΔP = the error in the location of point Q in the direction of the chord QR, i.e., the "derived" error, and

ΔS = the change in the length of QR due to panel deformation.

Therefore

$$\sigma_\delta^2 = \sigma_t^2 + \sigma_p^2 + \sigma_s^2 \tag{5.9}$$

where σ_t, σ_p, and σ_s are the standard deviations of ΔT, ΔP, and ΔS, respectively.

The line of sight error Ω includes the error in the angle set by the theodolite, the reading error (observation error), and the rigging tolerance, that is

$$\Omega = \Delta \psi + \frac{\Delta R}{L} \tag{5.10}$$

where $\Delta \psi$ is the error in the angle in the line of sight, ΔR is the statistical sum of the rigging tolerance and the reading error and is measured normal to the line of sight, and L is the slope distance between the theodolite and the target. Therefore

$$\sigma_\omega^2 = \sigma_\psi^2 + (\sigma_r / L)^2 \tag{5.11}$$

The distribution, expected value, and standard deviation of the derived error ΔP may be established if the statistical properties of the error in the coordinates of the previously located target Q are known. If ΔT, ΔS, ΔR, and $\Delta \psi$ are assumed to be normally

distributed with zero mean values, then ΔP and consequently the error functions Δ and Ω would also have normal distributions with zero mean values. Therefore, the effective surface error E will be normal and will have a mean value of zero and a standard deviation given by Eqs. (5.7), (5.9), and (5.11).

Since the surface error E arises from a linear combination of a large number of sources of error, then, according to the central limit theorem, the distribution of E is approximately normal even if the distributions of the component variables are not normal.

5.3.3 Magnitude of Errors. The magnitude of the standard deviation of each source of error was calculated by assigning a frequency of occurrence to the expected errors. Assuming a normal Gaussian distribution for each source, the standard deviation was then easily established. For example, the standard deviation of rigging tolerance was obtained by assuming that 10 mils of error would occur at one percent frequency of occurrence. The following table lists each source of error that was included in this analysis, its magnitude and (where applicable) its frequency of occurrence, and its calculated standard deviation. Where peak values are listed, they are assumed to be three times the standard deviation.

Source	Magnitude and Description	Standard Deviation
1. Location of Splice Plate	analyzed previously [4]	0.0024 inches
2. Distance Between Targets	.005 inches peak	0.0017 inches
3. Instrument Error	2 seconds of arc, frequency = 1/20	1.0 second
4. Thermal Errors*	.010 inches peak	0.0033 inches
5. Rigging Tolerance	.010 inches, frequency = 1/100	0.0037 inches

* Associated with rigging only

Based on these values, the expected rms of the effective surface error over the entire aperture due to the random sources is obtained as follows:

$$(rms)_r = \left[\frac{\int_A \sigma_\epsilon^2 \cdot f\,dS}{\int_A f\,dS} \right]^{\frac{1}{2}} = .0035 \text{ inches} \tag{5.12}$$

where the subscript r represents random sources. The significance of this number is shown in the next section.

5.4   RMS of Effective Surface Errors

The rms of the effective surface errors may be expressed as follows:

$$(rms)^2 = \frac{\int_A f\,(\epsilon + E)^2\,dS}{\int_A f\,dS} \tag{5.13}$$

where ϵ is the deterministic component of the effective surface error and E is its random component, which has a zero mean and a normal Gaussian distribution. The expected value of $(rms)^2$ may then be expressed by the following equation:

$$\overline{(rms)^2} = \frac{\int_A f\,(\epsilon^2 + \sigma_\epsilon^2)\,dS}{\int_A f\,dS} \quad , \tag{5.14}$$

since the expected value of the square of a normally distributed variant with zero mean is equal to its variance, that is

$$E^2 = \sigma_\epsilon^2 \;. \tag{5.15}$$

Then, the total rms may be presented as

$$\overline{(rms)^2} = (rms)_d^2 + (rms)_r^2 \tag{5.16}$$

where $(rms)_d$ is the deterministic rms of the reflector (Eq. (3.1)) and $(rms)_r^2$ is the average of the variance of the random component of the effective surface error over the aperture weighted by the illumination function (Eq. (5.12)).

Employing Eq. (5.16), the total expected rms of the rerigged reflector can be obtained.

32

5.5   Results and Conclusions

The final rms of the rerigged reflector, calculated on the basis of results of the night survey and on the assumption that only the inner panels are to be rerigged, is plotted in Fig. 23 for the range of zenith angle coverage. The rms ranges from a minimum of 16 mils to a maximum of 21 mils, at zenith angles of 50 degrees and 90 degrees respectively.

Noting that $(rms)_r$ was calculated in Section 5.3 to be 3.5 mils, it is apparent from Eq. (5.16) and Fig. 23 that the contribution of the random errors to the rms of the rerigged reflector is very small.

The average increase in the axial gain of the antenna, using Ruze's equation, is about 1.25 db at 15.75 GHz.

6. SUMMARY AND CONCLUSIONS

For the purpose of investigating the technical feasibility of rerigging the Haystack reflector, the following theoretical tools were developed:

1. A scheme was developed for the selection of an optimal sample of targets for predicting the error in the rms determination as affected by the size of sample.

2. Computer programs were written for processing and analysis of the optical surveys.

3. A statistical theory was derived for the prediction of surface deviations due to the random errors in the manufacture and rigging of the antenna.

4. A computer program was developed for the calculation of the radiation pattern of the reflector from the known surface errors.

5. An extension of Ruze's theory was developed for the prediction of the gain loss and scatter of reflectors with nonuniform error distributions.

Two samples of targets were selected for optical survey by Lincoln Laboratory, one consisting of 424 targets and the other of 212 targets. The 424-point survey was made at about midnight of 1 September 1966, and the 212-point survey during the early afternoon of 31 August 1966, a cloudy and mild summer day.

The rms of the reflector and the contour maps of its effective surface deviations were obtained from analyses of the two sets of optical measurements. The rms of the reflector in the face-up attitude was found to be about 37 mils for the night survey and 41 mils for the day survey. The larger surface errors(measured from the best-fit paraboloid) were found to occur in the region of the inner panels.

The gain and the half-power beamwidth corresponding to the measured surface deviations were calculated and compared with those obtained by radiometric measurements. Good agreement was obtained. Both the radiometric measurements and the analyses of the optical

measurements indicate a reduction in the half-power beamwidth as the axial gain decreases. This phenomenon is shown in Appendix A to be a characteristic of a reflector with its larger errors near the center.

A detailed analysis was made of the rerigged reflector, assuming that only the inner panels will be rerigged, and taking into account the effects of all the known deterministic errors and of the random errors from the initial rigging and the rerigging operation. It was found that the rerigged reflector will have an rms of about 16 to 21 mils, depending on zenith angle, and assuming thermal conditions similar to those of the night survey of 1 September 1966. This represents a reduction in rms of almost 50 percent.

Using Eq. (4.4), the average increase in the axial gain resulting from the rerigging is predicted to be about .36 db at 8.25 GHz and about 1.25 db at 15.75 GHz. The actual increase, however, is expected to be somewhat larger than these values, due to an expected increase in the size of the correlation region for the inner panels (see Eq. (9) of Reference 15). Another reason why Eq. (4.4) is expected to underestimate the increase in axial gain is associated with the fact that we have not taken into account the variability of radome blockage over the aperture. The effect of this blockage is to increase the relative influence of the inner panels, which, after rerigging, have considerably less error than the outer panels.

The half-power beamwidth of the rerigged antenna is expected to be somewhat larger than that of the present dish, since any reduction in errors in the central region of the reflector is expected to have the same effect as an increase in the taper of the illumination function and hence to increase the half-power beamwidth.

In the prediction of the surface deviations of the rerigged antenna, the errors due to the location of the theodolite were neglected. These errors can affect significantly the rms of

the rerigged reflector. To eliminate them, it is suggested that the rerigging be performed as follows:

1. Perform a survey of outboard targets with the theodolite located at some point near the RF axis. The process should include tape and angular measurements to selected splice plate targets and angular measurements to a sample of outboard targets.

2. Perform a computer analysis to establish the location of the theodolite with respect to the best-fit paraboloid through the measured outboard targets and obtain the angles for setting the inboard targets so that they will lie on the biased surface.

3. Perform the rigging of the surface in accordance with the rigging table generated above.

It should be noted that in this investigation the counterweight cable forces and the zenith angles at which they pick up load were assumed to remain unchanged. Obviously, some further level of improvement can be achieved if an investigation is performed to optimize the cable forces and their pick-up angles.

As was pointed out above, the predicted rms of 16 and 21 mils for the rerigged reflector assumes rather favorable nighttime conditions. Adverse thermal conditions can be expected to add roughly 4 to 8 mils to these values, depending on the effectiveness of environmental control measures.

On the basis of this investigation we conclude the following:

1. The validity of the theoretical formulations and analytical techniques which were developed is demonstrated by the good correlation between the analytical results and the radiometric measurements.

2. Rerigging of the Haystack antenna by adjustment of only the inner panels is feasible. The rms of the rerigged reflector under average thermal conditions is expected not to exceed 25 mils.

REFERENCES

1. Stuart, D. G., "Haystack, K & E Probe Calibration," Memorandum, M.I.T. Lincoln Laboratory, 25 February 1965.

2. Ruze, J., " Final Report - Haystack Rerigging Committee," Technical Memorandum No. 3L-0003, M.I.T. Lincoln Laboratory, 4 February 1966.

3. Zarghamee, M. S., Simpson, H., "Error Analysis of Haystack Antenna, Progress Report No. 1", Simpson Gumpertz & Heger Inc., 18 March 1966.

4. Zarghamee, M. S., Simpson, H., "Error Analysis of Haystack Antenna - Stochastic Approach, Report No. 2", Simpson Gumpertz & Heger Inc., 21 July, 1966.

5. North American Aviation Inc., "Bimonthly Status Report No. 22, For Contract AF19(604)-74000, Haystack Antenna System," Report No. NA61H-19-22, Section 3, July 1964.

6. Bourne, J. G., "Temperature Instrumentation of the Haystack Antenna-Radome and Dish," Report, Dynateck Corp.,18 June 1965.

7. Smith, H. D., Zarghamee, M. S., "Preliminary Report on Thermal Analysis of the Haystack Antenna," Memorandum, Simpson Gumpertz & Heger Inc., 9 September 1966.

8. Fisz, M., Probability Theory and Mathematical Statistics, John Wiley & Sons, Inc., New York, 1965, Chapter 14.

9. Simpson, H., Zarghamee, M. S., "Final Report - Analysis of 240- Point Survey of the Haystack Antenna," Memorandum, Simpson Gumpertz & Heger Inc., 29 June 1966.

10. Ruze, J., "Effective Surface Error Due to Rerigging Errors," Memorandum, M.I.T. Lincoln Laboratory, 10 November 1965.

11. Meeks, M. L., "Measured Gain Difference for the Haystack Antenna at 8 and 15.5 GHz," Memorandum, M.I.T., Lincoln Laboratory, 19 October 1966.

12. Allen, R. J., "Observations of Several Discrete Radio Sources at 3.64 and 1.94 Centimeters," Doctoral Thesis, Massachusetts Institute of Technology, December 1966.

13.   Ruze, J., Private Communication to M. S. Zarghamee, 3 February 1967.

14.   Simpson, H., Antebi, J., "Space Frame Analysis and Applications to Other Types of Structures," Presented at SHARE Design Automation Workshop, 24-26 June 1964.

15.   Ruze, J., "Antenna Tolerance Theory - A Review," Presented to 1965 International Symposium of the IEEE Groups on Antennas and Propagation.

APPENDIX A

A NOTE ON ANTENNA TOLERANCE THEORY

Deviations from the ideal paraboloid shape of antenna reflectors may be caused by manufacturing and rigging tolerances and by gravity, wind, and thermal effects. The effects of manufacturing tolerances, rigging tolerances, and errors in the instruments employed in the manufacturing and rigging process can be estimated at each point of the reflector through stochastic analyses [4]. Automated computation techniques permit structural engineers to predict the deformations of the reflector surface caused by known wind and gravity loads and temperature changes with a very good degree of accuracy [14].

To predict the loss of gain and pattern degradation due to surface errors, J. Ruze [15] proposed a formula in which a single quantity, namely the root mean square of the effective surface deviations, is employed as a measure of surface deviation from an ideal paraboloid shape. (Effective surface deviation is defined as one-half the change in the RF-path length and is equal to the axial component of the normal deviation from the best-fit paraboloid.) In his formulation, the assumption was made that surface deviations at any point on the reflector are random samples from a single normal Gaussian distribution with zero mean and a standard deviation equal to the rms error of the surface. These errors were further assumed to be correlated in small regions.

The actual effective surface deviations of a reflector may have a distribution which differs significantly from the above assumption. It is of interest to determine the range of validity of Ruze's equation in predicting the loss of axial gain and the change in the half-power

beamwidth for a reflector with nonuniform distribution of surface deviations.

In this appendix a general formula for the gain is developed and the accuracy of Ruze's equation is discussed. Finally a correction term is proposed which takes into account the effect of distribution of error over the aperture.

The gain of an aperture with a phase error $\delta\,(r,\,\varphi')$ may be expressed by the following equation:

$$G\,(\theta,\,\varphi)\ =\ \frac{4\,\pi}{\lambda^2}\ \frac{\left|\int_A\ f\,(\bar{r})\ e^{i\,\bar{k}\cdot\bar{r}}\ e^{i\,\delta\,(\bar{r})}\ dS\,\right|^2}{\int_A\ f^2\,(\bar{r})\ dS} \tag{A.1}$$

where $\quad\bar{r}\quad=\quad(r,\,\varphi')$ is the aperture position vector,

$\qquad\qquad f\quad=\quad$ the illumination function,

$\qquad\qquad\bar{k}\quad=\quad\dfrac{2\pi}{\lambda}\ \bar{p}_o\quad$ where $\bar{p}_o$ is a unit vector in the direction of observation, and

$\qquad(\theta,\varphi)\ =\quad$ the angular position of vector $\bar{k}$ (see Fig. 17).

Consider the phase error function δ at point $\bar{r}$ as a random sample from a normal Gaussian distribution with zero mean and a standard deviation $\sigma\,(\bar{r})$, a function of position within the aperture. Let us furthermore assume that the surface is subdivided into N regions; within each region the variance of phase error is so correlated that for the difference in the phase errors of points $\bar{r}_1$ and $\bar{r}_2$ in that region, we can write

$$\sigma^2\,(\bar{r}_1\,-\,\bar{r}_2)\,=\,[\,\sigma^2\,(\bar{r}_1)\,+\,\sigma^2\,(\bar{r}_2)\,]\,(1\,-\,e^{-\tau^2/c^2}) \tag{A.2}$$

where τ is the distance between $\bar{r}_1$ and $\bar{r}_2$ and c is the radius of the correlation region.

For N large, the expected gain of the antenna may be expressed as follows:

$$G(\theta,\varphi) = \frac{4\pi}{\lambda} \frac{\left| \int_A f(\bar{r}) e^{-\sigma^2/2} e^{i \bar{k}\cdot\bar{r}} dS \right|^2}{\int_A f^2(\bar{r}) dS}$$

$$+ \left(\frac{2\pi c}{\lambda}\right)^2 \sum_{n=1}^{\infty} \frac{1}{nn!} e^{-\left(\frac{\pi c u}{\lambda}\right)^2/n} \frac{\int_A f^2(\bar{r}) e^{-\sigma^2}(\sigma^2)^n dS}{\int_A f^2(\bar{r}) dS}$$

(A.3)

where $u = \sin\theta$. The coherent and incoherent parts reduce to the corresponding terms in Ruze's equation if $\sigma(\bar{r})$ is assumed to be constant over the aperture.

To compare the results of the above equation with those of Ruze's equation, the gain of a 120-foot antenna was calculated for a uniform illumination and with various distributions of the standard deviation of the phase error function over the aperture. For the purposes of this presentation, only the coherent part of the power is considered. The function $\sigma(\bar{r})$ is assumed to be radially linear and expressible as follows:

$$\sigma(\bar{r}) = \sigma_o + \nu(r - C_o)$$

(A.4)

where the constant σ_o is the rms of the phase error, ν is a measure of deviation of σ from σ_o and the constant C_o is chosen so that the following relation would hold:

$$\sigma_o^2 = \frac{\int_A \sigma^2(\bar{r}) dA}{A}$$

(A.5)

Two limiting conditions can be visualized; one where $\sigma(\bar{r})$ vanishes at the center, where $\nu = \sigma_o/C_o$ and another when $\sigma(\bar{r})$ decreases linearly and vanishes at the outer edge ($r = R$), where $\nu = \sigma_o/(C_o - R)$. For σ expressed by Eq. (A.4), the former value of ν corresponds to the maximum rate of increase of the standard deviation of the phase error and is thus referred to as ν_{max}; the latter corresponds to the minimum value of this rate of increase, and is referred to as ν_{min} (a negative quantity). Two intermediate conditions,

41

namely $\nu_1 = \nu_{max}/2$ and $\nu_2 = \nu_{min}/2$ are also considered. The variation of axial gain with the wave length is shown in Fig. 25 for various values of rms.

For the cases examined, a point of interest is that Ruze's equation always underestimates the gain. The deviation between the "actual" gain and that predicted by Ruze's equation increases for higher frequencies. A statistical proof of this statement in the general case is presented later in this appendix.

The increase in scatter with an increase in the rms error may be predicted by Ruze's equation. For this purpose a size must be assumed for the correlation region c. (A correlation radius of $c = D/20$ was assumed by Ruze.) An increase in the scatter, and thus in the half-power beamwidth, can be obtained by assuming larger correlation radii. The regional variation of the variance of the phase error over the aperture may be conceived of as a large underlying correlation region. It is therefore expected that the variation in σ^2 would affect the scatter significantly.

For the two limiting cases of radially linear variation of σ, namely for ν_{max} and ν_{min}, the half-power beamwidth is calculated as a function of the rms error σ_o of the reflector. The computation was performed for a uniformly illuminated circular aperture of 120-foot radius and $c = 5.6$ feet. The results are shown in Fig. 26.

It can be observed that the half-power beamwidth is significantly affected by the distributivity of the variance of phase error. For antennas having less error at the center, the half-power beamwidth is significantly greater than that predicted by the Ruze theory. When an antenna has its greatest surface deviations at the center, the half-power beamwidth decreases with increasing rms. This phenomenon may be explained by noting that as the central region deteriorates, the antenna tends to behave as an annular ring, whose half-power beamwidth decreases with an increase in the rms of the reflector.

The complexity of Eq. (A.3) reduces its suitability for use in approximate design. Certain simplifications will be made in this equation for this purpose. However, these simplifications limit the applicability of the theory to the prediction of the loss of gain alone. To predict the scatter, Eq.(A.3) must still be employed.

Considering only the first term of Eq. (A.3), the gain of the antenna can be written in the following form:

$$G(\theta,\varphi) = \frac{4\pi}{\lambda^2} e^{-\sigma_o^2} \frac{\left| \int_A f(\bar{r}) e^{-\xi/2} e^{i \bar{k}\cdot\bar{r}} dS \right|^2}{\int_A f^2(\bar{r}) dS} \tag{A.6}$$

where $\xi = \sigma^2(\bar{r}) - \sigma_o^2$, and σ_o^2 is the averaged variance of the phase error defined as follows:

$$\sigma_o^2 = \frac{\int_A \sigma^2(\bar{r}) f(\bar{r}) dS}{\int_A f(\bar{r}) dS} \tag{A.7}$$

Note that the average of ξ over the surface is zero. Therefore, if we assume that ξ at each point on the aperture is a random sample from a normal Gaussian distribution with zero mean and standard deviation σ_ξ, then the expected value of gain can be written as follows:

$$G(\theta,\varphi) = G_o e^{-\sigma_o^2} e^{\sigma_\xi^2/4} \tag{A.8}$$

To express the above equation in terms of surface deviations, let us introduce the rms of the effective surface deviations defined as follows:

$$\epsilon_o^2 = rms^2 = \frac{\int_A \epsilon^2 f(\bar{r}) dS}{\int_A f(\bar{r}) dS} \tag{A.9}$$

where the function ϵ is the effective surface deviation from the best-fit paraboloid for deterministic errors and it is the standard deviation of the effective surface deviations for random errors. Let us also define a quantity called the second variance of surface

deviations as follows:

$$\eta_o^4 = \text{second variance of surface deviations} = \frac{\int_A (\epsilon^2 - \epsilon_o^2)^2 \, f(\bar{r}) \, dS}{\int_A f(\bar{r}) \, dS} \qquad \text{(A.10)}$$

Then, Eq. (A.8) may be written as follows

$$G = G_o \, e^{-(\frac{4\pi \, \epsilon_o}{\lambda})^2} \, e^{\frac{1}{4}(\frac{4\pi \, \eta_o}{\lambda})^4} \qquad \text{(A.11)}$$

A comparison of this equation with Eq. (A.3) and Ruze's equation is made in Fig. 27 for the case of radially linear variation of the effective surface deviations. The results indicate the range of validity of Ruze's equation and the level of improvement that can be achieved by employing the modified equation, Eq. (A.11).

It can easily be observed from Eq. (A.11) that if η_o does not vanish, then the gain predicted from Eq. (A.11) is always larger than that predicted from Ruze's equation. That is, the Ruze theory always underestimates the gain of the antenna for a given rms of effective surface deviations.

APPENDIX B

PROGRAM BESTFIT

B.1   Introduction

The program BESTFIT was written primarily for the analysis of the optical survey of the Haystack reflector. Employing the zenith angles of the selected targets, the program computes the effective surface deviations (with respect to the best-fit paraboloid) and the rms of the reflector for any desired position of the antenna. The program is written in FORTRAN for the CDC 3300 computer.

The solution process involves computing the surface deviations with respect to an initial reference paraboloid. This reference paraboloid is then shifted as a rigid body and its focal length is changed so as to obtain the minimum rms. The corresponding effective surface deviations and the rms of the reflector are then calculated. These best-fit surface deviations are augmented by the dead weight travels of the antenna in going from zero to a desired zenith angle and the best-fitting process is repeated. The program also generates the input for programs CONTOUR and RADPAT.

In the following sections, the input and the output of this program are described in detail. The limitations and the restrictions of the program are also discussed. The terminology used is described below.

A Real Set consists of the surveyed targets on a single radial target line.

A Dummy Set consists of the non-surveyed targets on a single radial line. Since the program assumes that a target is located at every intersection of a circumferential row and a radial line, some dummy targets are imaginary.

Target Index Number (T.I.N.) is an index which sequentially numbers all circumferential rows (see Figure 28).

Target Sequence Number (T.S.N.) is.an index which sequentially numbers the circumferential rows on which one or more surveyed targets are located (see Fig. 28).

Target I.D. is the identification for a target. It specifies the target row, the panel number on which the target is located, and whether the target is an edge target or a center target (i.e. H24C).

B.2   Input

The input to this program consist of the coordinates of each radial line of targets, the measured zenith angles, the measured or expected errors in the distances between targets and in the radii of the splice plate targets, the area-illumination factor associated with each target, and the dead weight displacements in the face-up and face-side attitude. The input is prepared in fourteen blocks as described below:

BLOCK I   Coordinates of Inboard Targets (10X, 2F12.6)

ID	RIN(J)	ZIN (J)

ID   =   Identification of the card. (This field will not be read by the computer.)

RIN(J)   =   Radius of the Jth inboard target in inches (J=T.I.N.).

ZIN(J)   =   Z-coordinate of the Jth inboard target in inches.

Note: There are a total of seven cards in this block, one for every circumferential row; they must be arranged in order of ascending T.I.N.'s. The splice plate target row is included both here and in BLOCK II.

BLOCK II   Coordinates of Outboard Targets (10X, 2F12.6)

ID	ROUT (J)	ZOUT (J)

ROUT(J) =   Radius of the Jth outboard target in inches.

ZOUT(J) =   Z-coordinate of the Jth outboard target in inches.

Note: BLOCK II is similar to BLOCK I except for the number of cards, which is nine in this block. The splice plate target row is included both here and in BLOCK I.

46

BLOCK III Program Constants (2I5, F12.6)

NLINE	LLINE	F

NLINE = Total number of real sets and dummy sets.

LLINE = Total number of real sets.

F   = Design focal length of the antenna in inches.

BLOCK IV Distance Errors (10X, 9F7.4)

ID	DIST (I,1)	DIST (I,2)	/ DIST (I,N)

DIST(I,1)= Distance error between the best-fit axis of revolution and the splice plate target of the Ith real set in inches.

DIST(I,J)= Distance error between targets T.S.N. = J and T.S.N. = J + 1.

Note: There are a total of LLINE cards, which may be arranged in any arbitrary manner; however, their order must be the same for BLOCKS V, IX, XI, XII, and XIII.

BLOCK V Area-Illumination Factors (8X, 9F8.5)

ID	AR (I,1)	/ AR (I,N)

AR(I,J) = Area-illumination factor associated with the target T.S.N. = J of the Ith real set.

BLOCK VI Controlling Indices (3I5)

NIN	NOU	NTRAV

NIN   = The highest T.S.N. of the inboard targets.

NOU   = The highest T.S.N. of the outboard targets.

NTRAV = 0 if antenna is in face-up attitude,

       = 1 if antenna is not in face-up attitude.

BLOCK VII   <u>Inboard Target Sequence</u> (715)

INX(1)	INX(2)	//	INX(7)

INX(I)   =   T.S.N. of the Ith inboard target.

BLOCK VIII   <u>Outboard Target Sequence</u> (915)

IOX (1)	IOX (2)	//	IOX (9)

IOX(I)   =   T.S.N. of the Ith outboard target.

BLOCK IX   1. <u>Set Controls</u> (A4,6X,2I5)

KLINE (I)	NDD (I)	ICK (I)

KLINE(I)=   INBO   This indicates that the Ith set is an inboard set.

         =   OUTBD   This indicates that the Ith set is an outboard set.

NDD(I)   =   The line number on which the Ith set is located.

ICK(I)   =   0   if the Ith set is real,

        =   1   if the Ith set is a dummy set.

2. <u>Zenith-angle Measurements</u> (A1,F2.0,A1,4X, F4.0,2F3.0)

TARG	θ_1	θ_2	θ_3

TARG   =   Target I.D.

θ_1 , θ_2 , θ_3 =   The zenith angle measured to the target under consideration in degrees, minutes, and seconds, respectively

Note: Part 2 is omitted for dummy sets.
            Block IX is repeated for all real and dummy sets.

NOTE: BLOCKS X thru XIII are required only when NTRAV = 1; that is when the antenna is not in face-up attitude.

BLOCK X   <u>Antenna Position</u> (8X, F8.5)

ID	POS

POS   =   Zenith angle of antenna in degrees

48

BLOCK XI   Face-up Deflections (19X, 3E13.5)

ID	DISX (I,J)	DISY (I,J)	DISZ (I,J)

$\left.\begin{array}{l} DISX(I,J) \\ DISY(I,J) \\ DISZ(I,J) \end{array}\right\}$ = x,y, and z displacements of the target T.S.N. = J of the Ith real set due to dead loads when antenna is in the face-up position (in inches).

There are NIN or NOU cards in this block. They must be arranged in the ascending order of the T.S.N.s.

Note: Repeat this block for each real set.

BLOCK XII   Face-side Deflections (19X,3E13.5)

ID	AISX (I,J)	AISY (I,J)	ASIZ (I,J)

This block is similar to BLOCK XI except that these displacements are due to dead loads when antenna is in the face-side position.

Note: Repeat this block for each real set.

BLOCK XIII   Center Cable Displacements (19X, 3E13.5)

ID	C2X (I,J)	C2Y (I,J)	C2Z (I,J)

Similar to BLOCK XII except that these displacements are due to the action of the center cable.

Note: Repeat this block for each real set.

BLOCK XIV   Controls (2I5)

NWI	NTRAV

NWI   =   0   Terminates the run.

       =   1   Returns control to Block X.

NTRAV =   0 or 1, as defined in Block VI.

NOTE: Repeat BLOCKS X and XIV for other desired position angles if the BLOCKS XI, XII, and XIII have already been read in the computer. Otherwise, repeat BLOCKS X thru XIV.

49

B.3   Output

The output of this program includes most of the input data; the location of the theodolite; the effective surface errors with reference to the best-fit paraboloid at the surveyed targets; the best-fit rms of the reflector weighed by the area-illumination factors, and an input data deck to the CONTOUR program for plotting the isograms of the effective surface deviations.

The various sections of output are listed below:

BLOCK I	Input BLOCKS I thru IX are printed.
BLOCK II	The elevation angle of the antenna.
BLOCK III	The location of the theodolite relative to the best-fit paraboloid.
BLOCK IV	The effective surface error with respect to the best-fit paraboloid and the area-illumination factors associated with each surveyed target.
BLOCK V	The best-fit root mean square of the effective surface error of the reflector weighted by the area-illumination factors.
BLOCK VI	The best-fit rms of the effective surface errors of the reflector with all the area-illumination factors equal to unity.
BLOCK VII	NR, the number of targets located on a radial line including the targets in both real and dummy sets; NT, the number of radial lines.
BLOCK VIII	The radii of each target row.
BLOCK IX	The circumferential angle of each radial line.
BLOCK X	The effective surface errors with respect to the best-fit paraboloid for all real and dummy targets. As a contour plotting aid, the effective surface errors at dummy targets are obtained by linear interpolation between the values at the adjacent real targets.
NOTE	BLOCKS I thru VI are printed, BLOCK VII is punched, and BLOCKS VIII thru X are printed and punched. BLOCK I is printed only once; all the other blocks are generated for every desired position angle of the antenna. (The punched data is used as input to program CONTOUR.)

B.4   Restrictions and Remarks

This program was designed mainly for the analysis of survey measurements of the Haystack antenna. It was not attempted to make the program completely general for direct application to any other reflector. However, there are only two sections in this program which are not applicable to other problems, and they can be modified to fit almost any problem with little effort. These two sections are as follows:

1.   The target identification system. The target identification is used to locate a target and to obtain its coordinates. Any change in the target identification system requires a corresponding change in the program.

2.   The dead load displacements due to the deflection compensation cables. For problems which have no deflection compensation cable systems, the user can provide a dummy set of input data. Even for Haystack antenna, if the elevation angles at initial cable pick up are changed, the program must be appropriately modified.

The program employs essentially the full core storage (32,768 storage locations). Therefore, in addition to the restrictions mentioned above, the following size limitations must be observed:

NIN   ≤   7

NOU   ≤   9

LLINE   ≤   56

NLINE   ≤   80

Total number of lines ≤ 40

Total number of measured targets ≤ 440

The program uses standard input and output units.

B.5   Running Time

The approximate running time of this program is about three minutes for the first zenith angle and slightly less than two minutes for each successive value.

51

APPENDIX C

PROGRAM CONTOUR

C.1   Introduction

For a function F defined at all the nodes of a polar grid system, the program CONTOUR can be employed to obtain a contour plot of the variation of F over any annular region. The program can employ unequal grid intervals and produces the isograms of $F(r,\varphi')$ at specified intervals. This program is written in FORTRAN language for the CDC 3300 computer with an attached display unit.

The program CONTOUR consists of a main program, the three subroutines CONTACT, MODE, and CONNECT, and a number of plotting subroutines provided by the present library routines of the CDC 3300 computer at Haystack Hill, Westford, Mass. The main program controls the input phase and the calling sequence of the various subroutines. The subroutine CONTACT searches the array $[A_{ij}]$ and locates all the equipollent points by linear interpolation between the elements of the array, and it determines the points to be connected together to form an isogram. The subroutine MODE determines whether the beginning point and the end point of an isogram should be connected together. The subroutine CONNECT converts the polar coordinates of the equipollent points to the cartesian coordinates and then plots the isograms.

C.2   Input

The input to the program CONTOUR includes two vector arrays containing the radii and the circumferential angles of the node points of the grid, the array $[A_{ij}]$ containing the values of the function F at the node points, the maximum and the minimum isogram intensities to be plotted, the interval between isograms, and the title to be printed on the contour plot.

It is important to note that the input to this program may be obtained from the program BESTFIT with the exception of isogram control cards and the identification card. A detailed description of the input to this program is given below.

BLOCK I   Define Grid System (2I5)

| NVROW | NVCOL |

NVROW   =   The number of nodes on a radial line = the number of rows of matrix A.

NVCOL   =   The number of nodes on a circumferential line = the number of columns of matrix A.

BLOCK II   Define Grid Radii (8F10.4)

| R (1) | R (2) ⟩ ⟨ R (8) |

R (I)   =   The r-coordinate of the Ith radial node in inches.

Note: There are NVROW nodes on a radius; they must be read in numerical order.

BLOCK III   Define Circumferential Angles of Grid (6F12)

| THETA (1) | THETA (2) ⟩ ⟨ THETA (6) |

THETA (J) =   θ-coordinate of the Jth node on a circumferential line, in radians.

Note: There are NVCOL joints on a circumferential line; they must be arranged in numerical order.

BLOCK IV   Values of Array [A] (6F12)

| A (I,1) | A(I,2) ⟩ ⟨ A(I,J) |

A (I,J)   =   The value of the function F defined at a node located on the Ith radial line and the Jth circumferential line.

BLOCK V   Contour Control (3F12.6)

S1	S2	S3

S1   =   The lowest isogram value to be plotted.

S2   =   The highest isogram value to be plotted.

S3   =   The interval between isograms.

See Note (5) under Remarks.

BLOCK VI   Identification (20A4)

IIE

IIE   =   The title of the plot.

The title appears at the bottom of the plot.

NOTE: Repeat Blocks I thru VI for next problem. If there are no more problems to be done, provide a blank card to terminate the run.

C.3   Output

The output of this program is a contour plot which is shown on the display unit. A 35mm snapshot is automatically taken of each plot. Also, the machine pauses after each plot is completed and types "PLEASE TAKE PICTURE" on the console typewriter, to permit a Polaroid photograph to be taken.

All input data as well as the location designations of the first point and the last point of each isogram is printed for checking purposes.

C.4   Remarks

This program was designed for plotting the effective surface deviations of the Haystack reflector. There are certain sections in the program which may be modified, if desired,

without any difficulty. These are described below.

(1)   The inner boundary and the outer boundary of the reflector are plotted with
        radii equal to 60 inches and 720 inches respectively.

(2)   The θ (1) line is set to point to the north direction. The successive lines are
        assumed to be defined in the counterclockwise direction.

(3)   The maximum number of rows and columns of the matrix A is 16 and 65 respectively.

(4)   The total number of equipollent points of any single isogram cannot be greater
        than 400.

(5)   Since the isogram intensities are printed on the plot, it seemed desirable to
        multiply the elements of the input matrix by a factor of 100 to reduce the number of the
        printed significant digits. Input Block V should be specified with respect to the
        modified matrix. For instance, if the unit of the input matrix is in inches, S3 = 20
        means isograms are required at the interval of 0.2 inches. The intensities shown
        on the plot can have no more than three digits or two digits preceded by a minus
        sign. Fractions, if any, will not be shown on the plot.

APPENDIX D

PROGRAM RADPAT

D.1   Introduction

The program RADPAT computes the radiation diagram of an annular aperture whose surface deviations from a best-fit paraboloid are known. The half-power beamwidth can easily be obtained by manually plotting the output. The program has been written in FORTRAN language for the CDC 3300 computer.

The gain in a given direction of observation defined by φ and θ (Fig. 17) is expressed by the following equation:

$$G(\theta,\varphi) = \frac{4\pi}{\lambda^2} \frac{\left| \int_A f(\bar{r}) e^{j\bar{k}\cdot\bar{r}} e^{j\delta(\bar{r})} dA \right|^2}{\int_A f^2(\bar{r}) dA}$$

where

$$\bar{r}=(r,\varphi') \quad = \quad \text{the position vector, in polar coordinates, of a point on the aperture,}$$

$$\lambda \quad = \quad \text{the wave length,}$$

$$f(\bar{r}) \quad = \quad \text{the aperture illumination function,}$$

$$\delta(\bar{r}) \quad = \quad \text{the phase error } = \frac{4\pi\epsilon}{\lambda} \text{ (ϵ is the effective surface deviation), and}$$

$$\bar{k} \quad = \quad \frac{2\pi}{\lambda} \hat{p} \text{ where } \hat{p} \text{ is a unit vector in the direction of observation.}$$

The illumination function is assumed to be axially symmetric and to have a paraboloid-on-a-pedestal distribution. The edge taper is arbitrary and is input by specifying the ratio of the value of the function at the edge of the aperture to the value at the center.

The integration is performed by assuming that the variation of the integrand between the nodes is expressible by a general second degree polynomial. The polynomial is then Integrated. This integration process is quite accurate and involves negligible discretization error.

56

The input to the program RADPAT includes the array $[A_{ij}]$ containing the values of the effective surface deviations defined at all the nodes of a polar grid system, the coordinates of the node points, the boundaries of the aperture, the increments of θ and φ for defining the radiation pattern, the wave length, and the illumination taper.

The input is described in detail in the following sections.

BLOCK I   Problem Identification (20 A4)

KD

. KD   =   The identification of the problem.

BLOCK II   Define Program Constants (4F10.6, I5, 2F10.6, I5, F10.6)

RR	RIN	ALFAB	ALFSTP	NALFA	TB	TSTP	NTS	GG

RR   =   The outer radius of the aperture in inches.

RIN   =   The inner radius of the aperture in inches.

ALFAB   =   The initial value of θ in degrees.

ALFSTP   =   The increment of θ in degrees.

NALFA   =   The total number of θ's.

TB   =   The initial value of φ in degrees.

TSTP   =   The increment of φ in degrees.

NTS   =   The total number of φ's.

GG   =   The ratio of edge-to-center value of illumination function.

BLOCK III   Define Grid System (2I5)

NR	NT

NR   =   The number of nodes on a radial line = the number of rows of matrix A.

NT   =   The number of nodes on a circumferential line = the number of columns of matrix A.

BLOCK IV   Define Grid Radii (8F10.4)

| R (1) | R (2) | } { | R (NR) |

R (I)   =   The r-coordinate of the Ith radial node in inches.

Note: There are NR nodes on a radial line, and they must be read in numerical order.

BLOCK V   Define Circumferential Angles of Grid (6 F12.6)

| THTA (1) | THTA (2) | \ { | THTA (NT) |

THTA (J) =   The θ-coordinate of the Jth node on a circumferential line in radians.

Note: There are NT nodes on a circumferential line, and they must be read in numerical order.

BLOCK VI   Define Matrix A (6F12.6)

| A (1,1) | A (1,2) \ { | A(I,J) |

A (I,J)   =   The value of the effective surface deviation of a node point located on the Ith radial line and the Jth circumferential line of the grid, in inches.

BLOCK VII   Define Wave Length (F12.6)

| AAMDA |

AAMDA =   The wave length in centimeters.

Repeat Block VII for different wave lengths.

BLOCK VIII   Initiate a New Problem or Terminate the Run

One blank card will instruct the machine to read input Blocks I thru Block VIII of a new problem. Two blank cards will terminate computer run.

D.3. Output

The output of the program consists of the identification of the problem, the wave length, and the values of gain. The values of gain in db are listed in a matrix form with different φ angles listed column-wise and different θ angles listed row-wise.

D.4 Size Limitations

The following size limitations should be observed

$$NR = 2n + 1; n \leq 8$$
$$NT = 2m; m \leq 32$$
$$NALFA \leq 20$$
$$NTS \leq 20$$

D.5 Running Time

The running time is approximately three seconds for the evaluation of a single value of gain for a grid having 700 nodes.
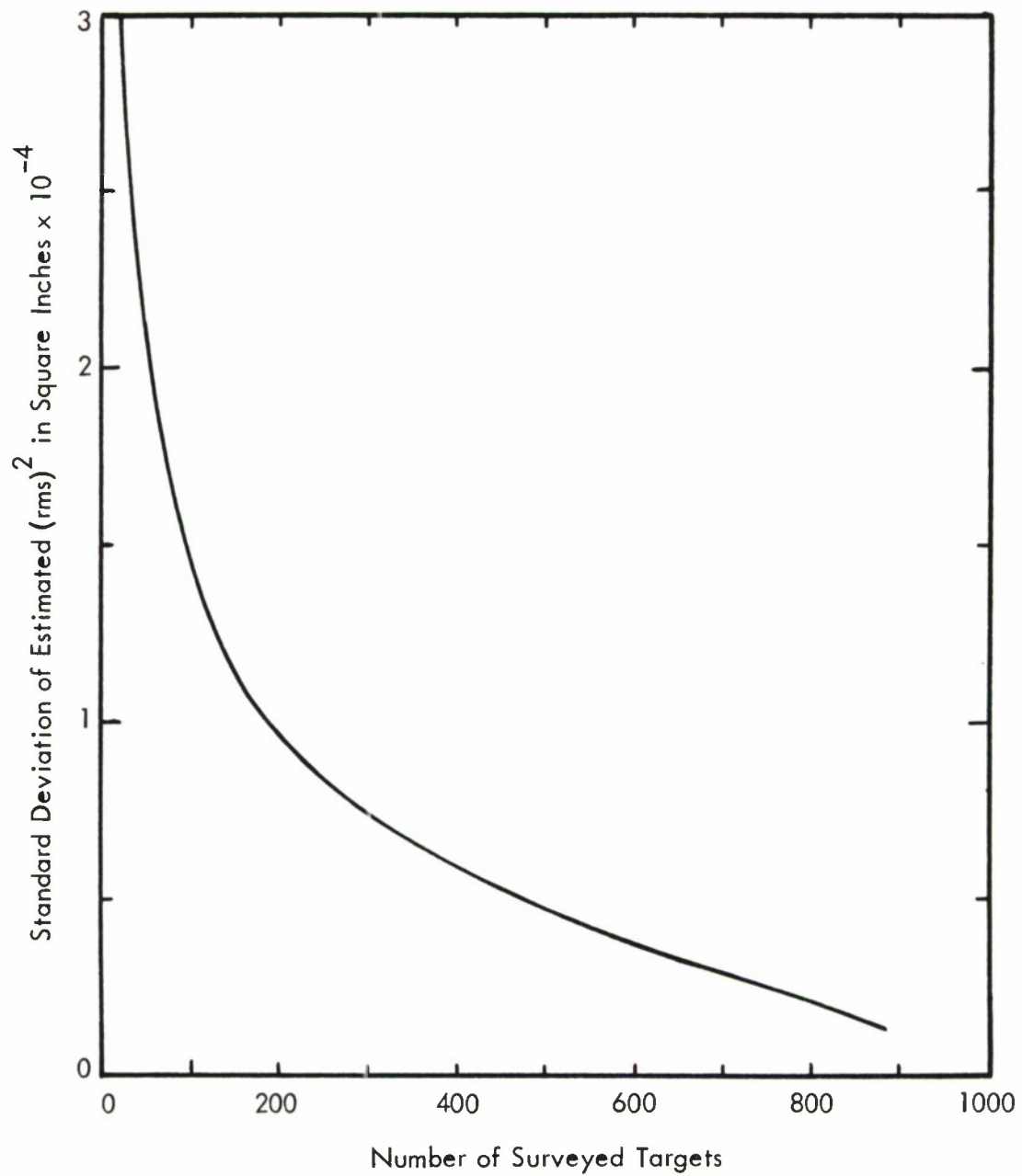
FIGURE 1 – VARIATION OF THE STANDARD DEVIATION OF THE
ESTIMATED $(RMS)^2$ OF THE REFLECTOR WITH THE
NUMBER OF SURVEYED TARGETS
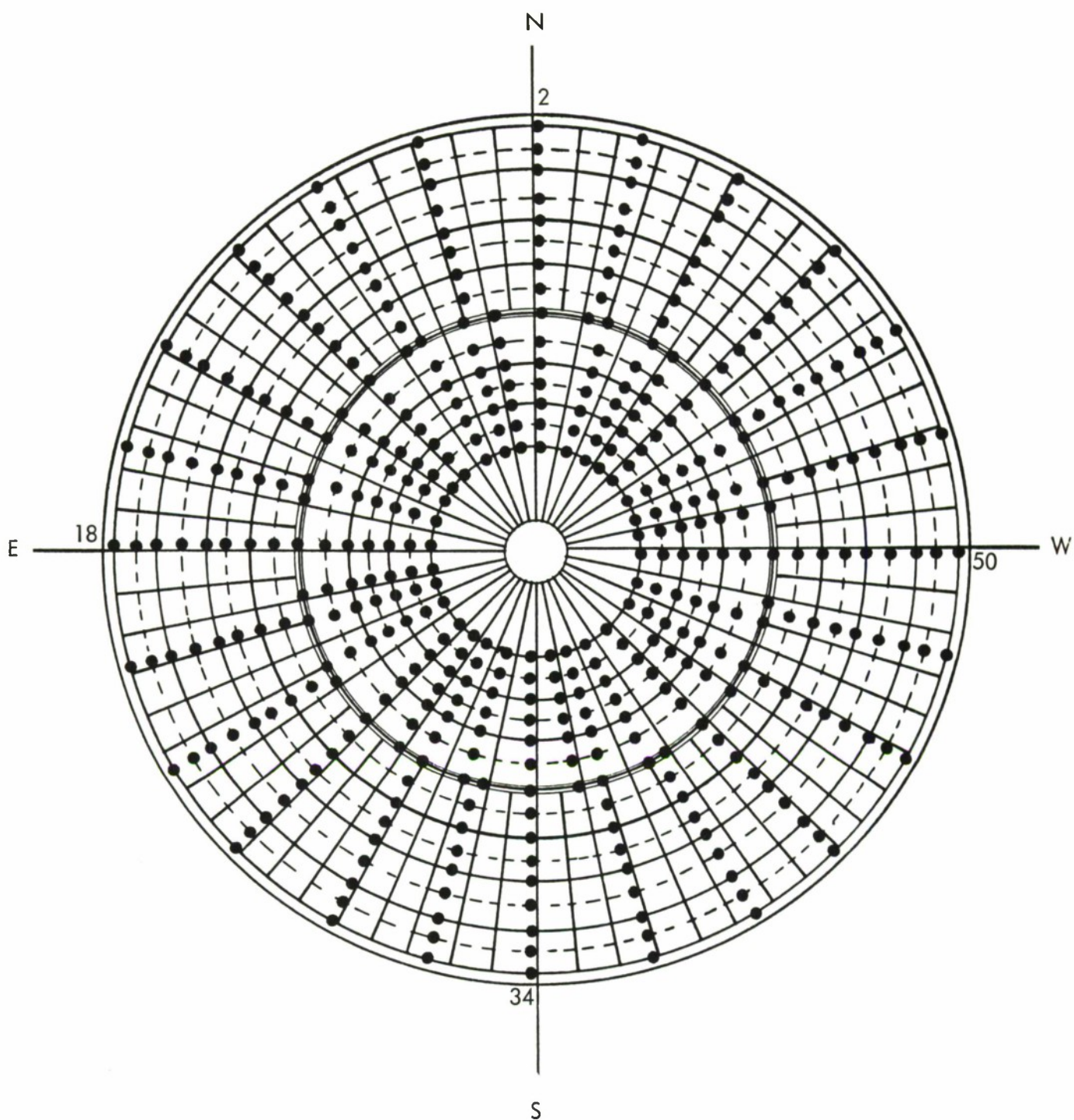
FIGURE 2 - LOCATION OF 424 TARGETS USED FOR NIGHT SURVEY
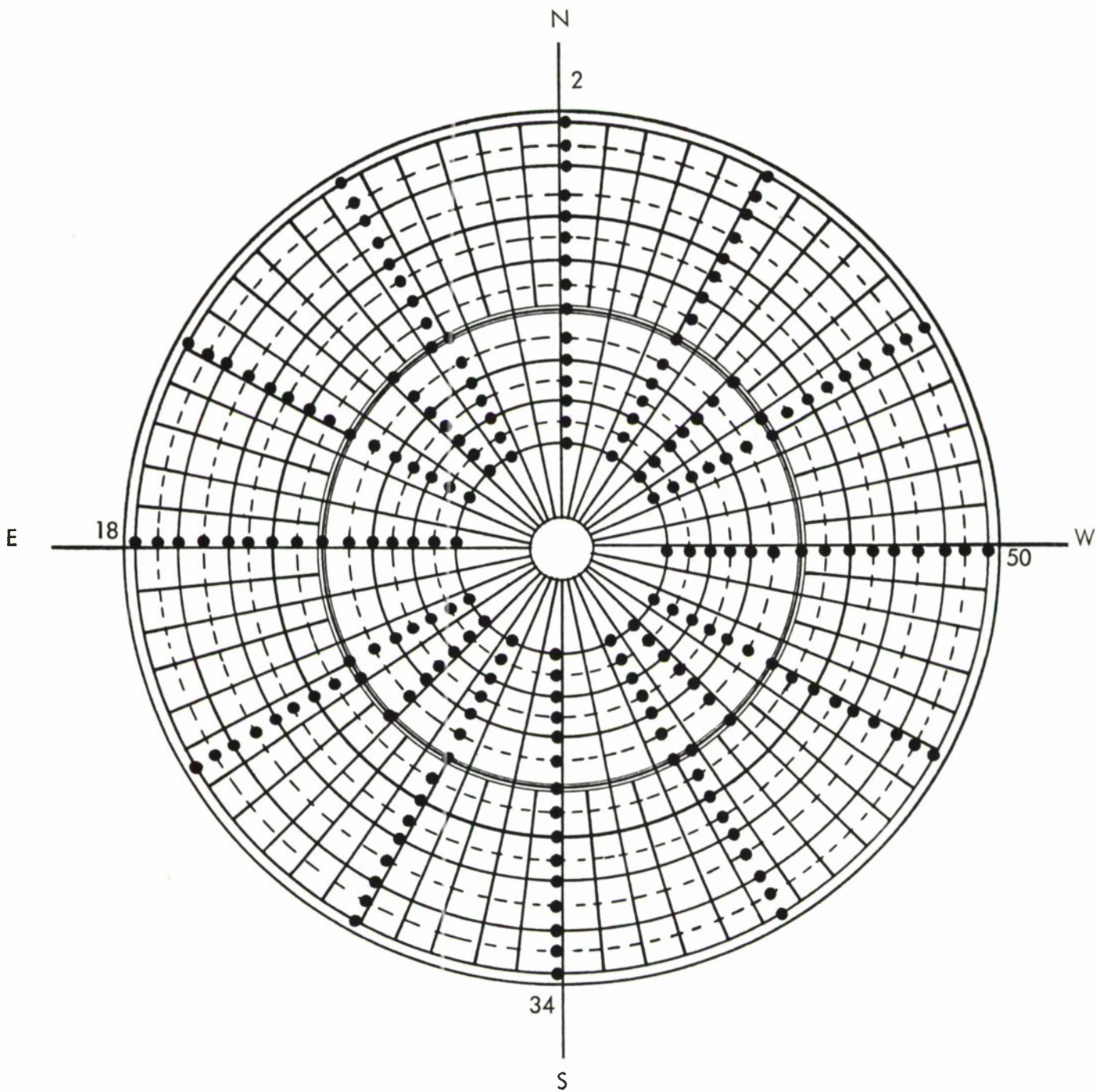
FIGURE 3 – LOCATION OF 212 TARGETS USED FOR DAYTIME SURVEY
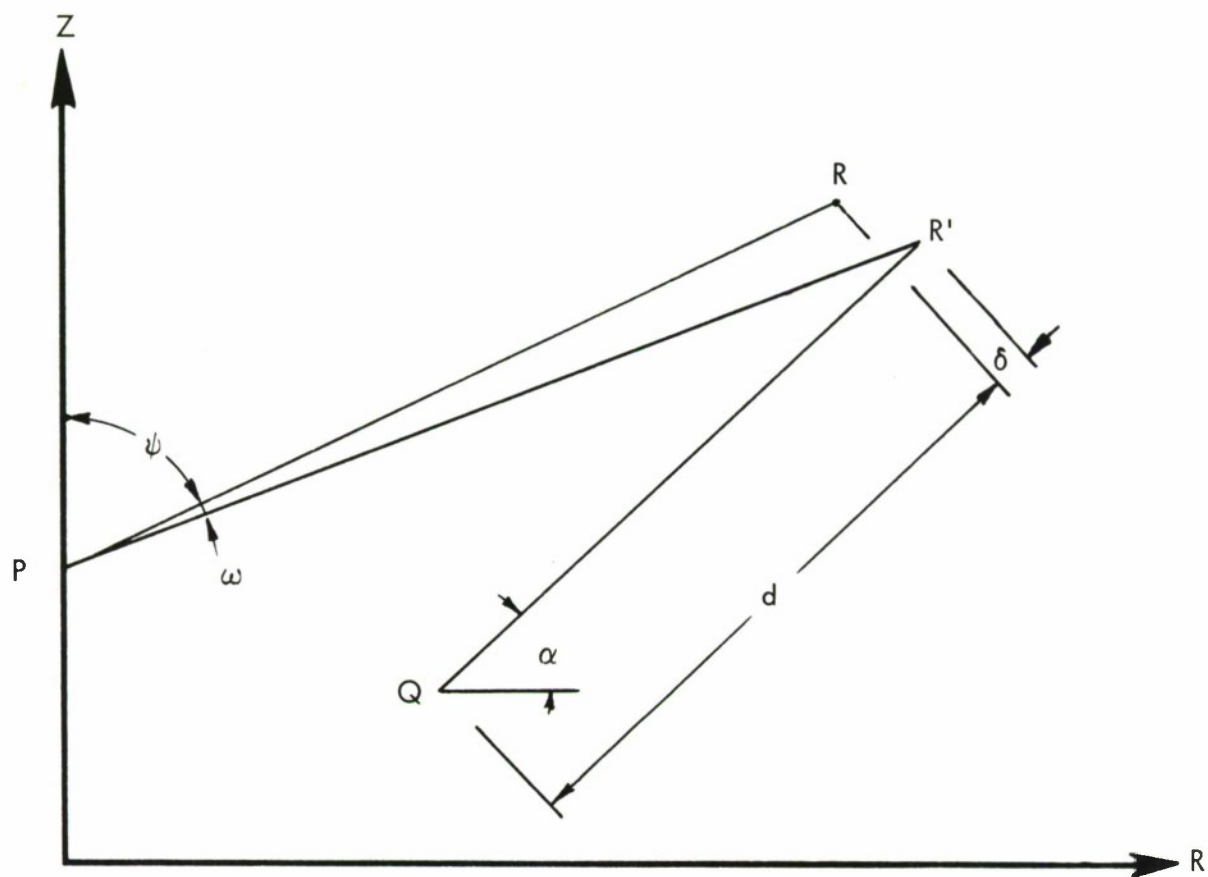
FIGURE 4 – NOTATION
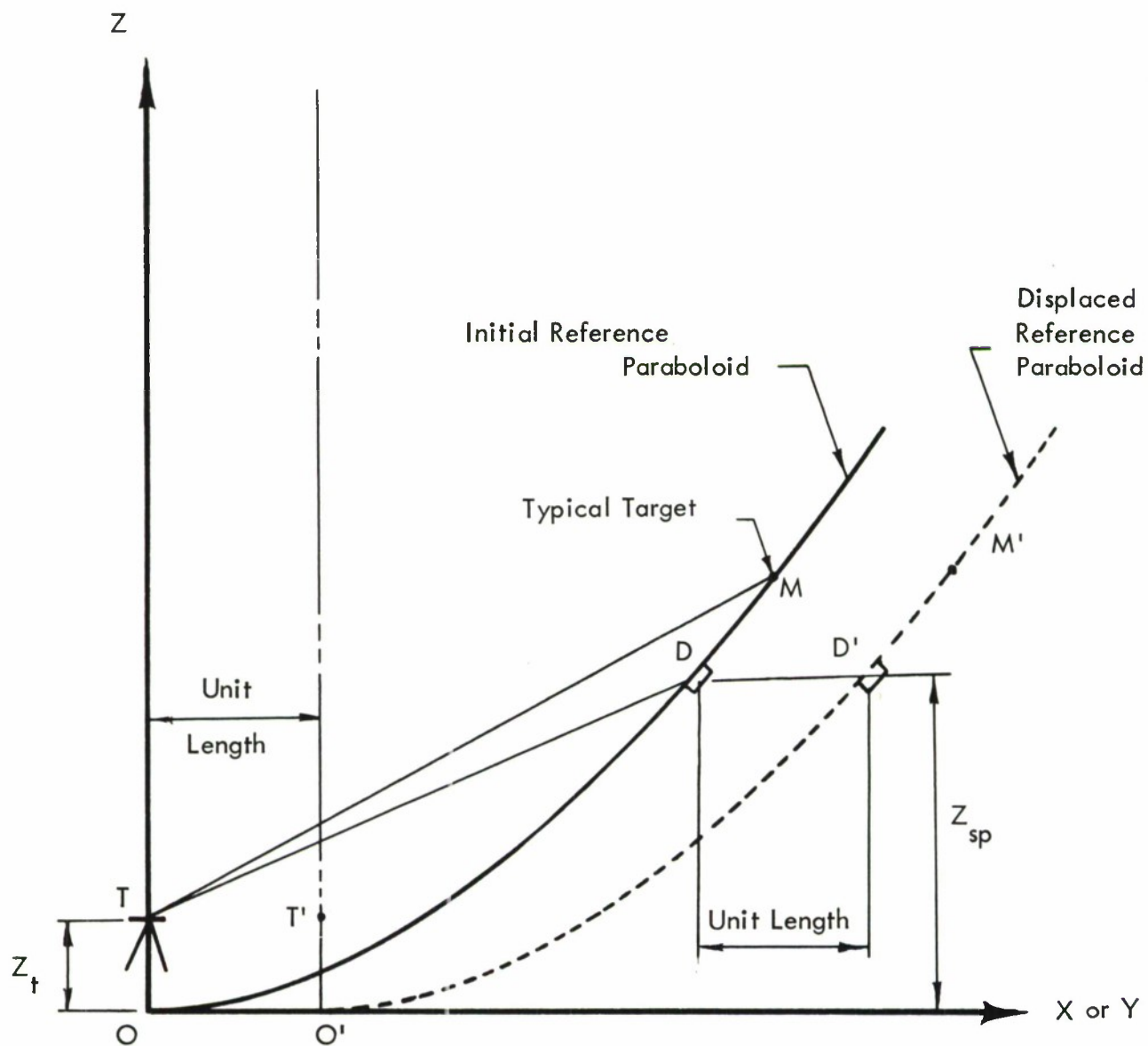
FIGURE 5 - EFFECT ON TARGET DEVIATION OF X- OR Y-DISPLACEMENT
OF INITIAL REFERENCE PARABOLOID
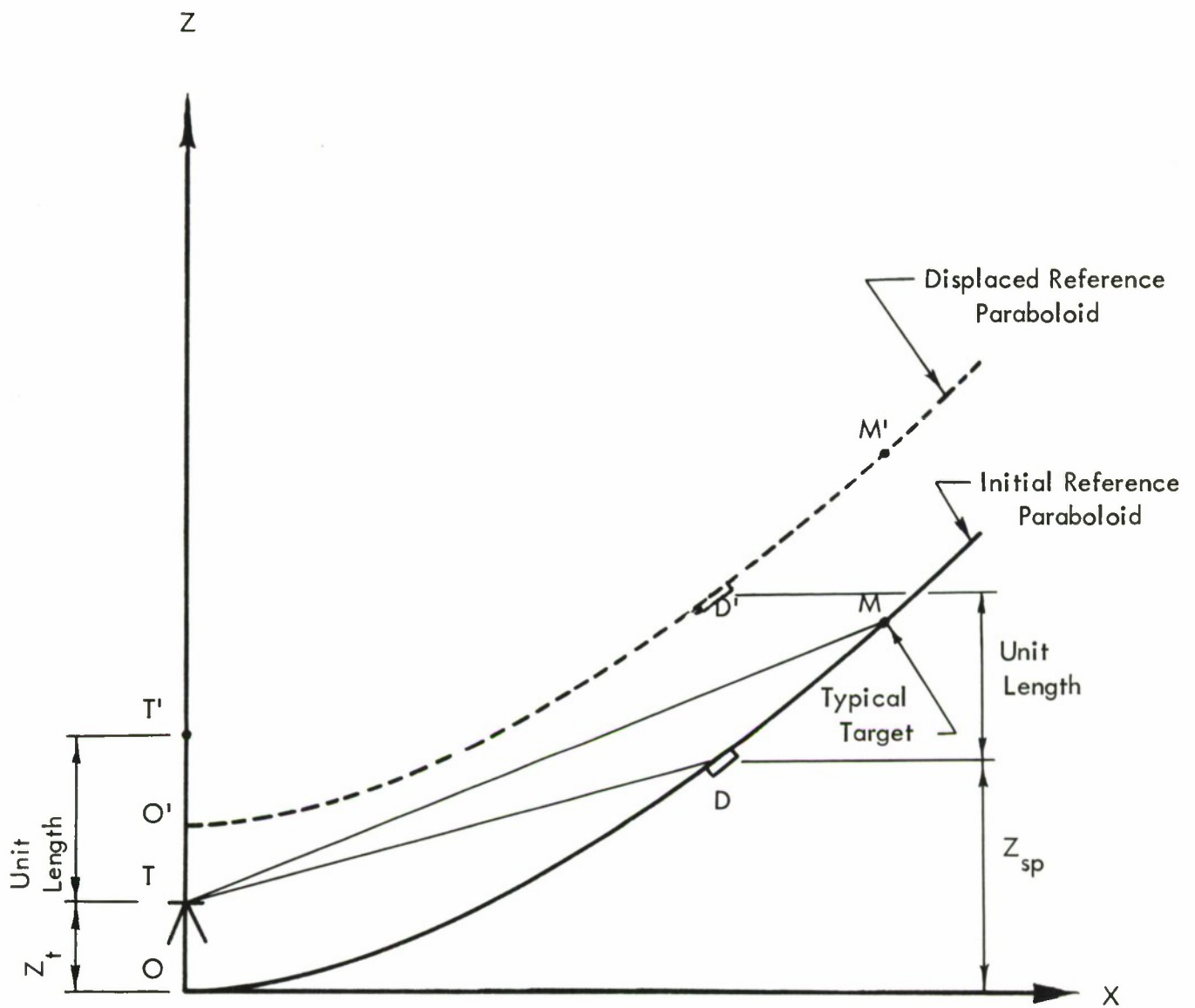
FIGURE 6 – EFFECT ON TARGET DEVIATION OF Z – DISPLACEMENT
OF INITIAL REFERENCE PARABOLOID

66
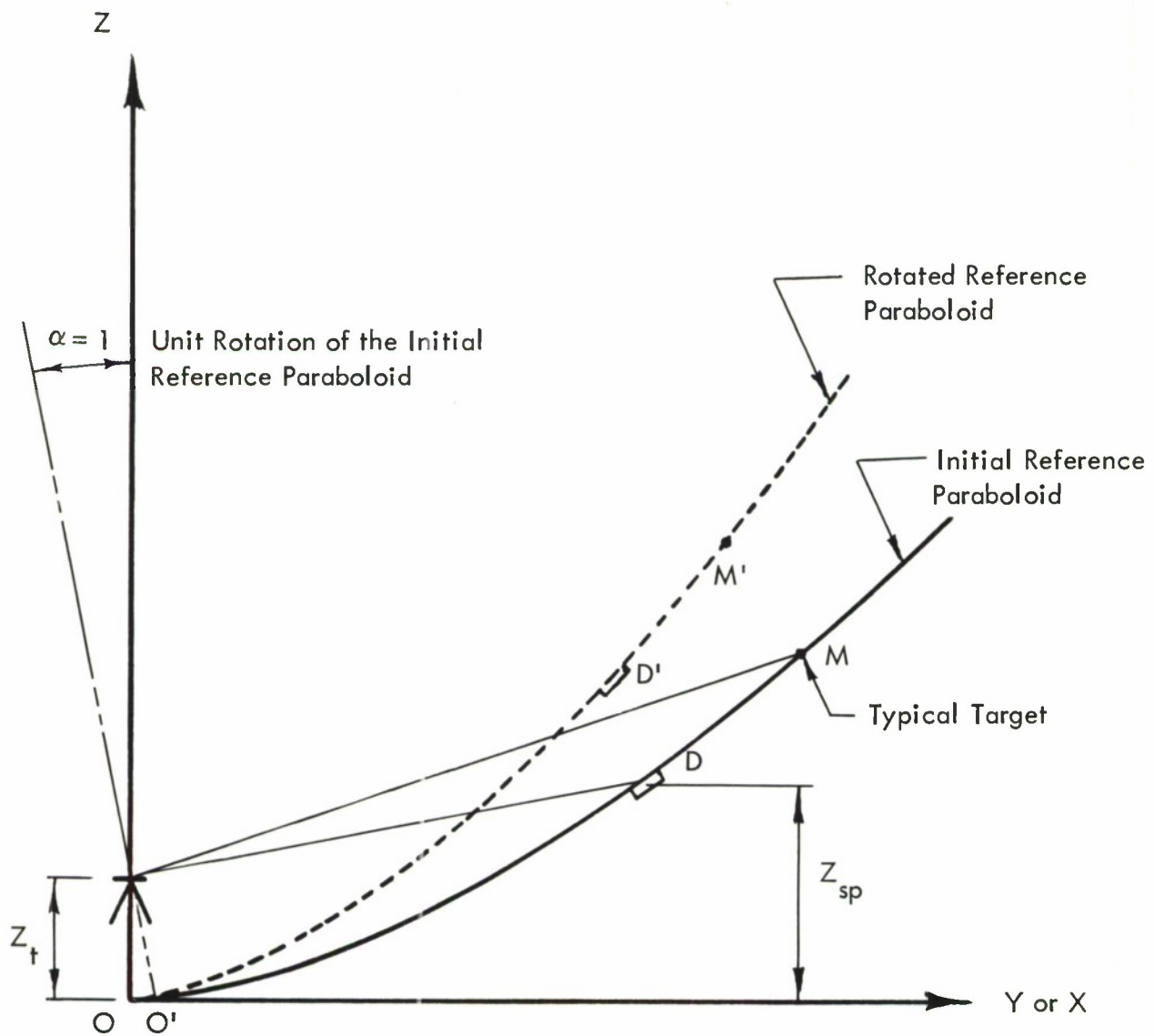
FIGURE 7 - EFFECT ON TARGET DEVIATION OF ROTATION OF
INITIAL REFERENCE PARABOLOID

Zenith Angle of Antenna in Degrees

RMS in inches
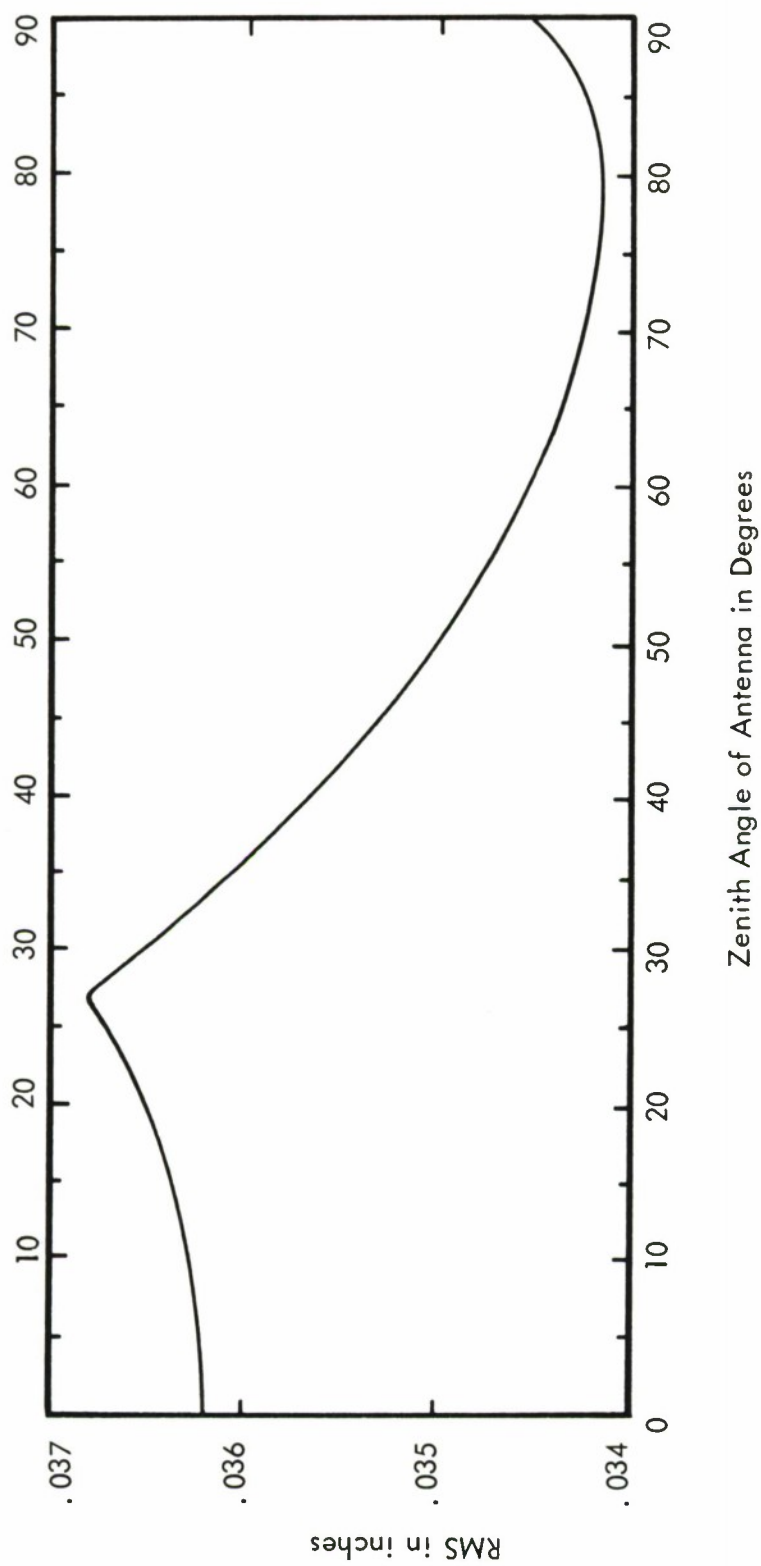
FIGURE 8 – VARIATION OF CALCULATED RMS WITH ZENITH ANGLE; NIGHT SURVEY; EDGE TAPER = 12db
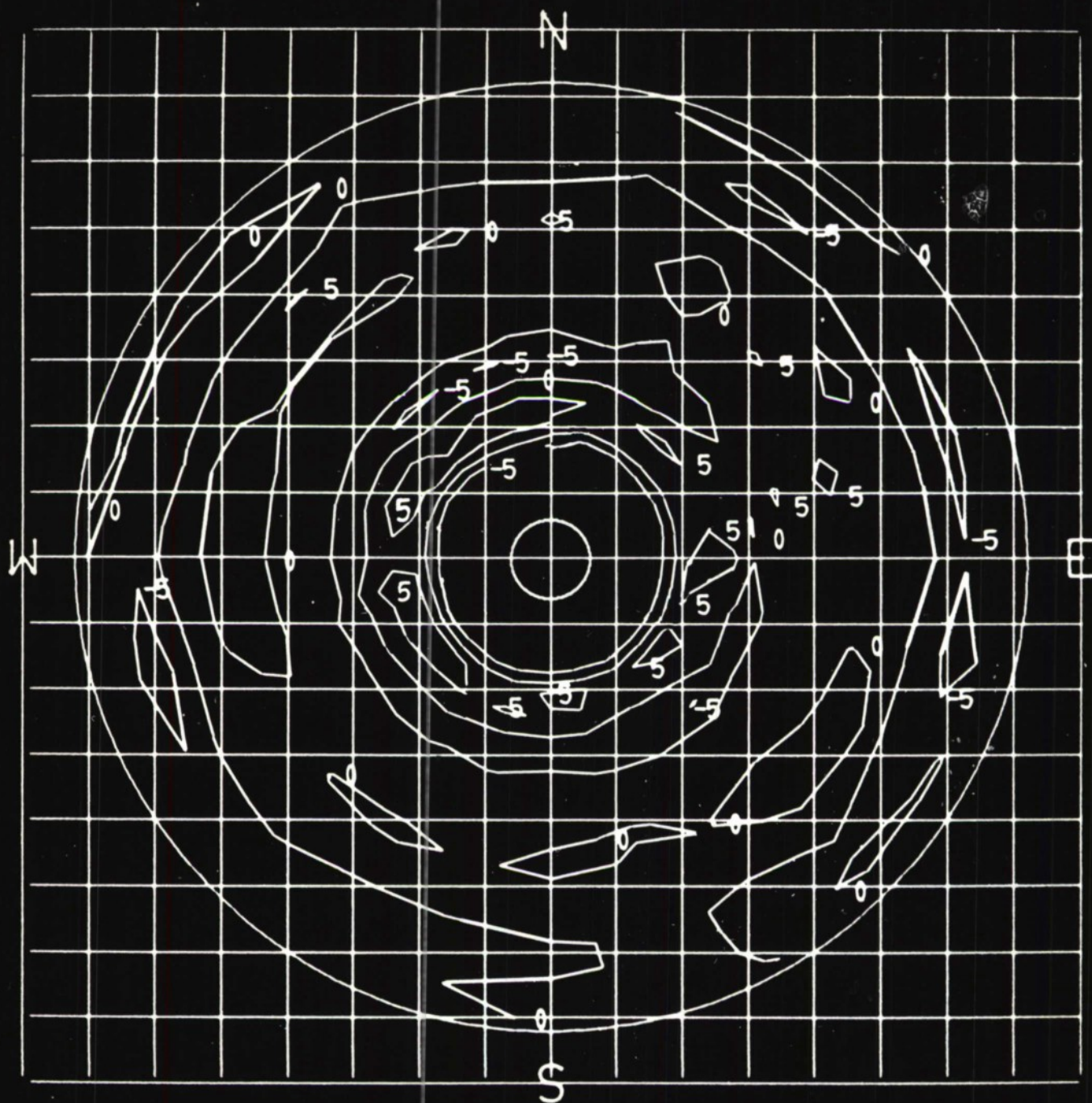
FIGURE 9 - CONTOUR MAP OF MEASURED EFFECTIVE SURFACE DEVIATIONS - NIGHT SURVEY
CONTOUR INTERVAL = 50 MILS; ZENITH ANGLE = 0 DEGREES
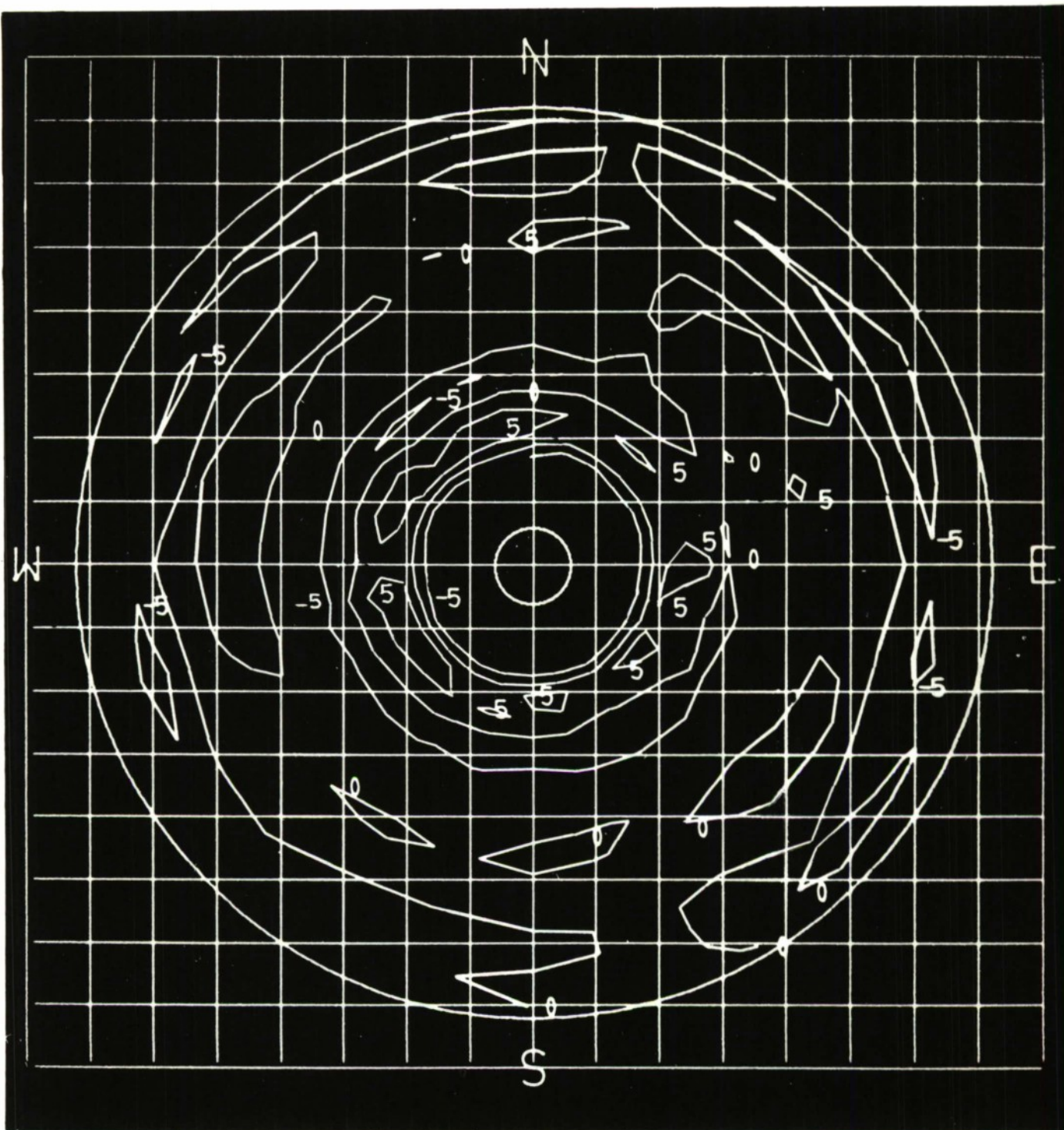
FIGURE 10 – CONTOUR MAP OF MEASURED EFFECTIVE SURFACE DEVIATIONS – NIGHT SURVEY

CONTOUR INTERVAL = 50 MILS; ZENITH ANGLE = 15 DEGREES
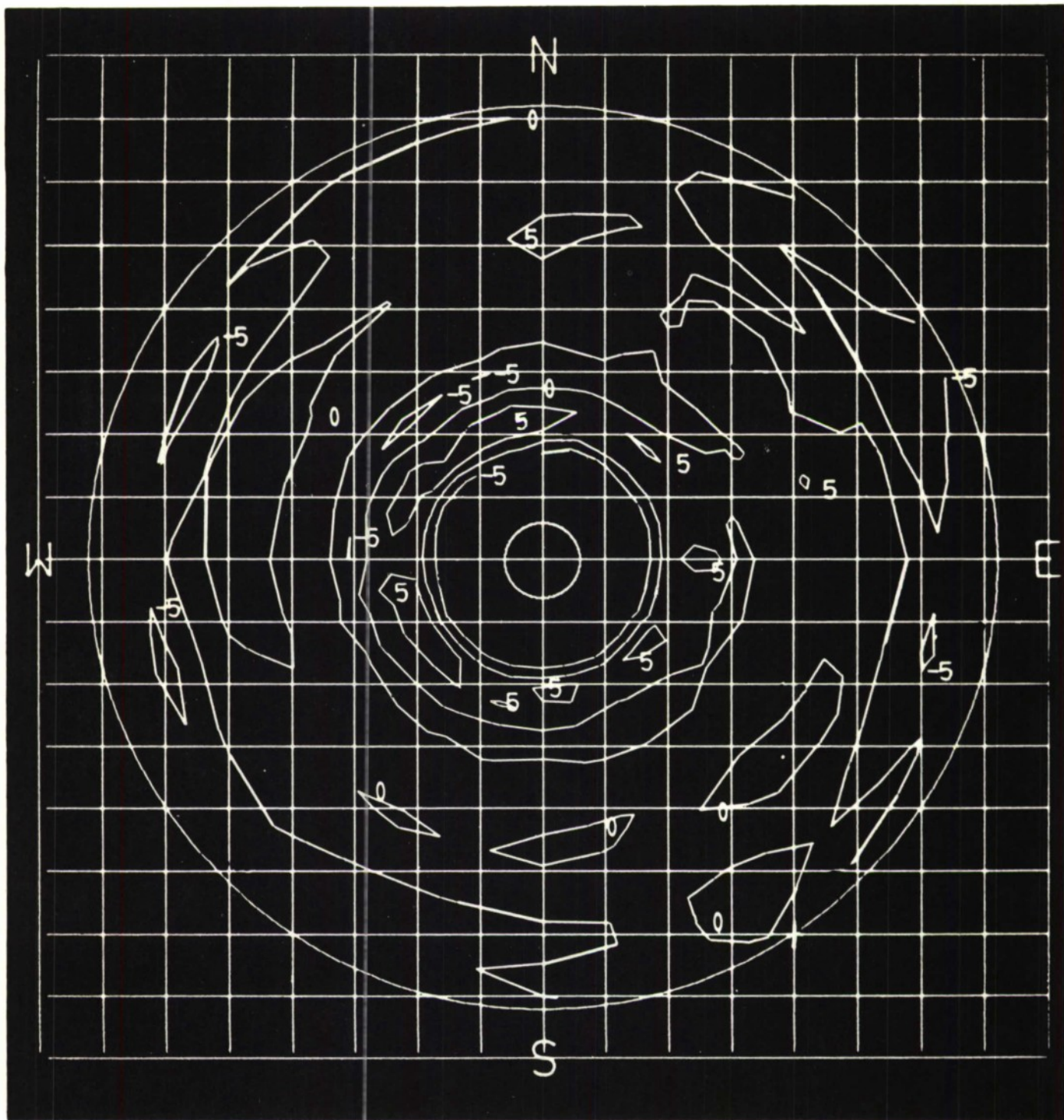
FIGURE 11 - CONTOUR MAP OF MEASURED EFFECTIVE SURFACE DEVIATIONS - NIGHT SURVEY
CONTOUR INTERVAL = 50 MILS; ZENITH ANGLE = 30 DEGREES
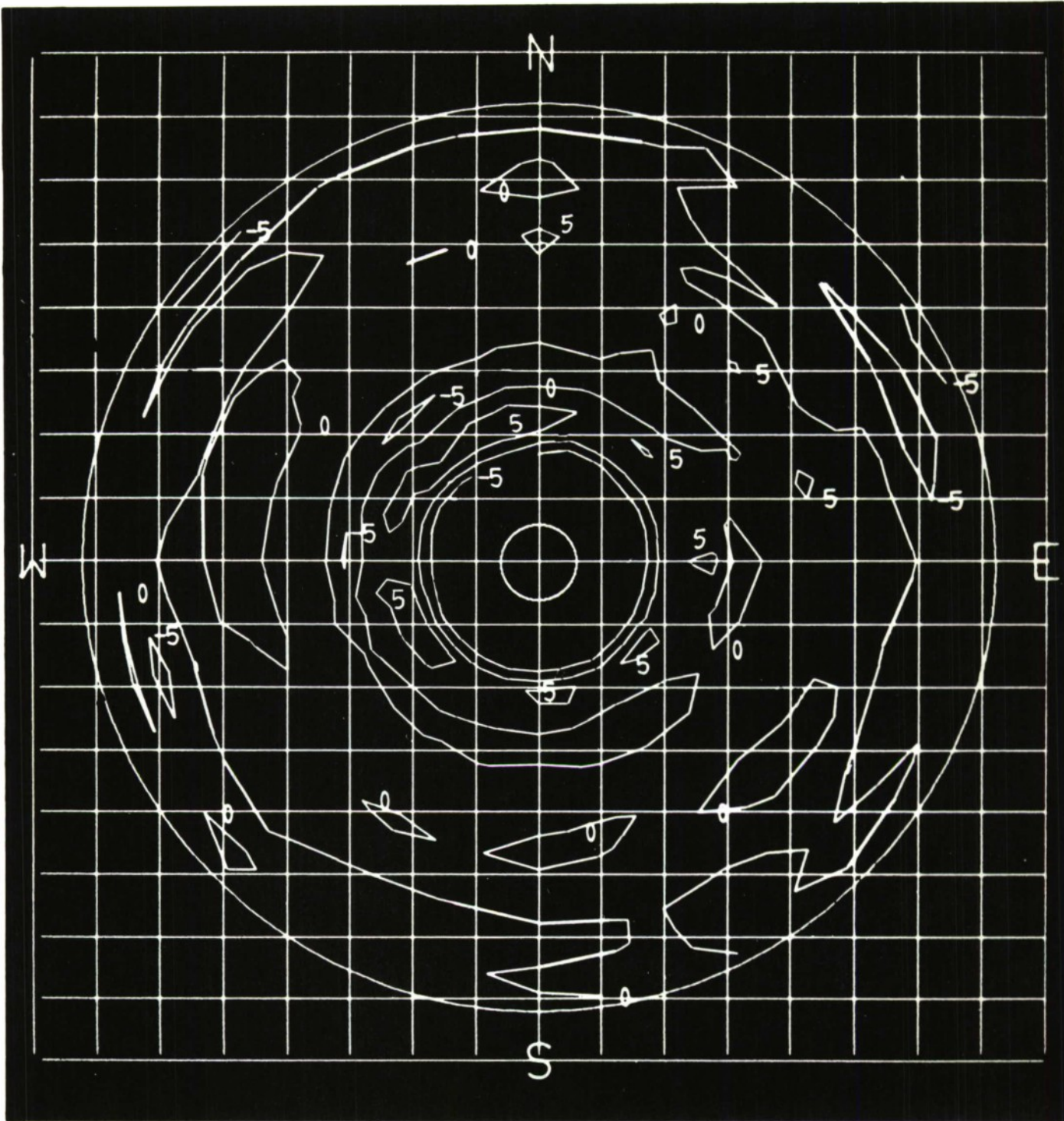
FIGURE 12 - CONTOUR MAP OF MEASURED EFFECTIVE SURFACE DEVIATIONS - NIGHT SURVEY
CONTOUR INTERVAL = 50 MILS; ZENITH ANGLE = 45 DEGREES
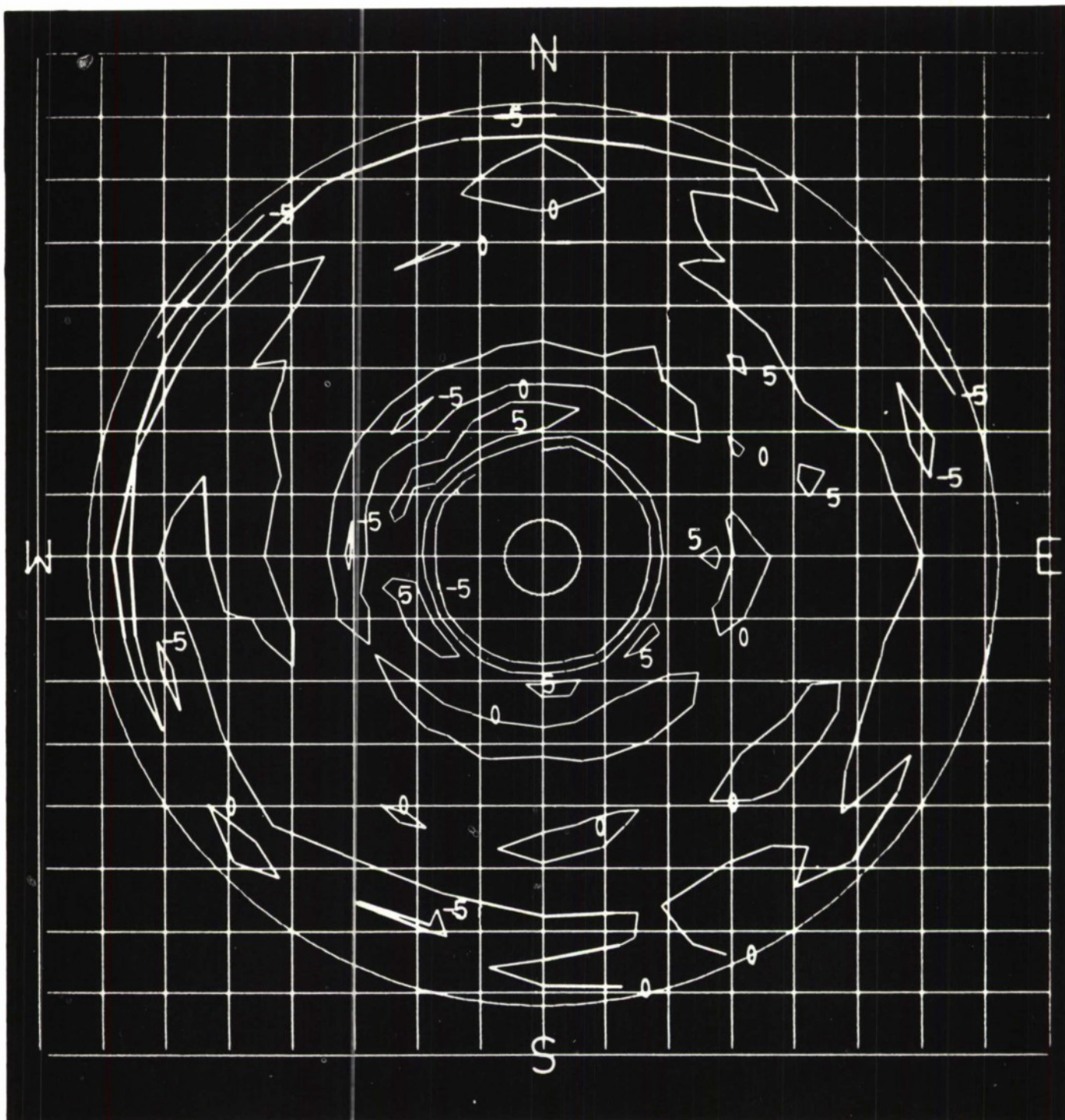
FIGURE 13 – CONTOUR MAP OF MEASURED EFFECTIVE SURFACE DEVIATIONS – NIGHT SURVEY
CONTOUR INTERVAL = 50 MILS; ZENITH ANGLE = 60 DEGREES
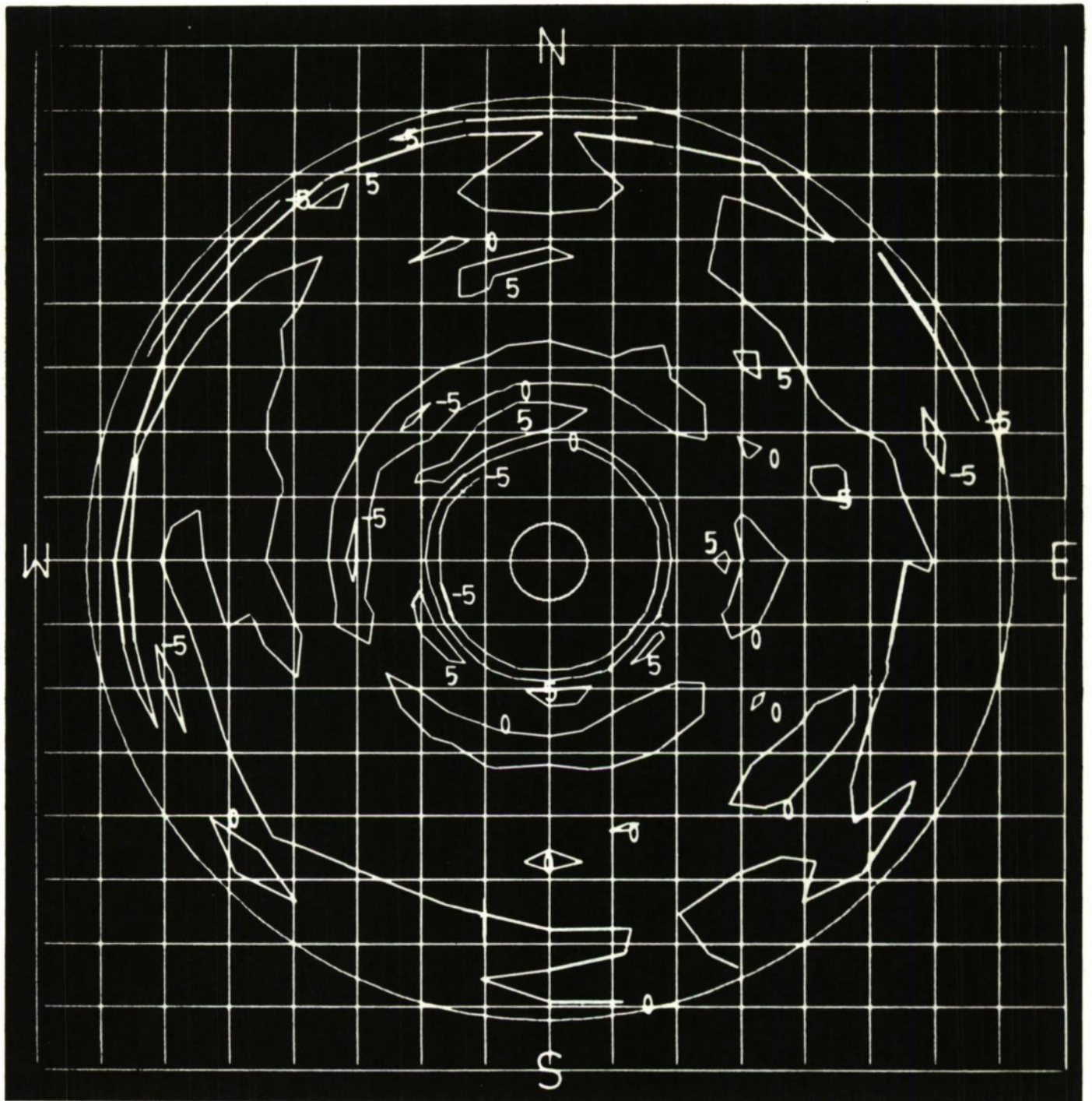
FIGURE 14 - CONTOUR MAP OF MEASURED EFFECTIVE SURFACE DEVIATIONS - NIGHT SURVEY
CONTOUR INTERVAL = 50 MILS; ZENITH ANGLE = 75 DEGREES
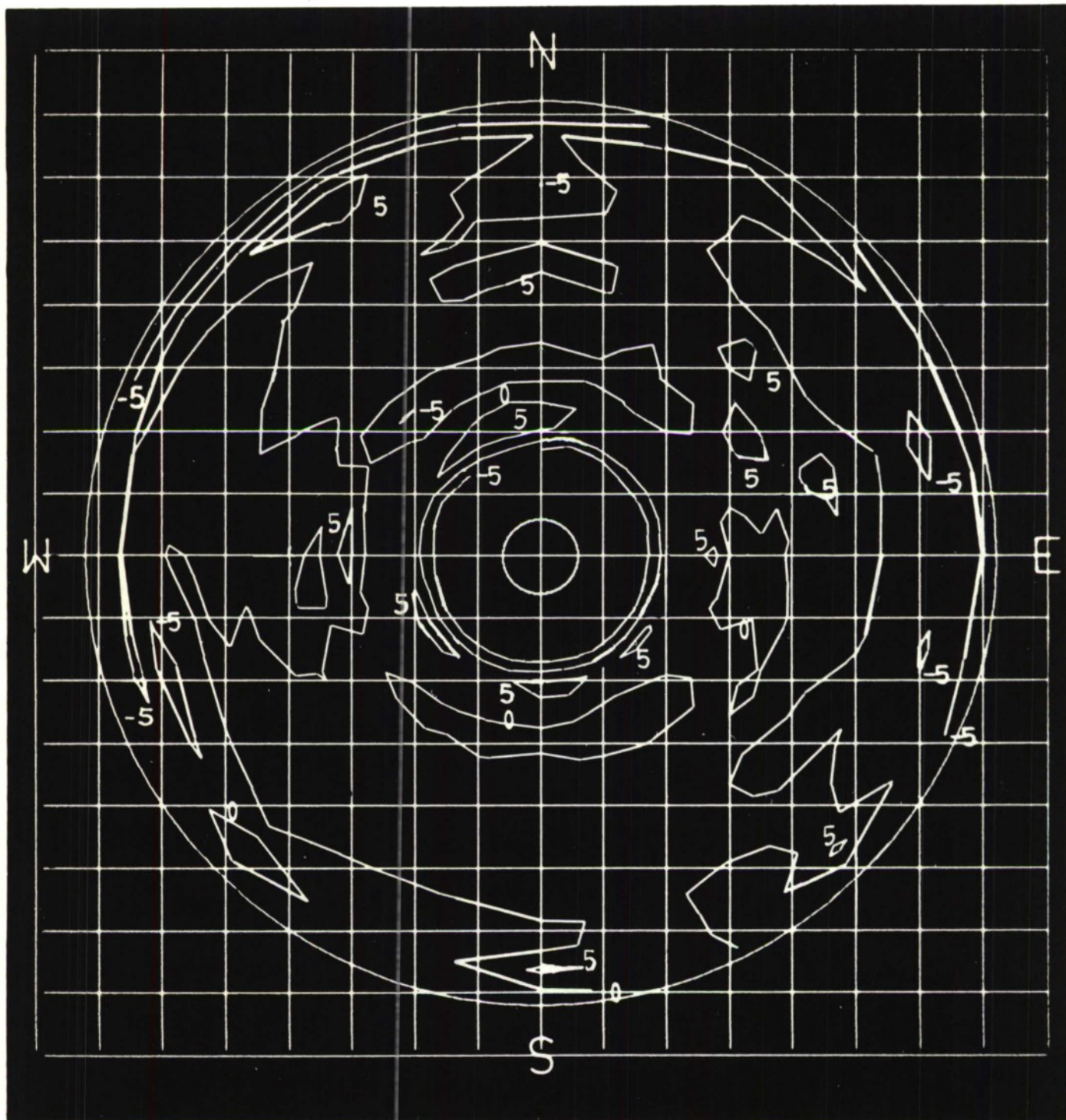
FIGURE 15 - CONTOUR MAP OF MEASURED EFFECTIVE SURFACE DEVIATIONS - NIGHT SURVEY
CONTOUR INTERVAL = 50 MILS; ZENITH ANGLE = 90 DEGREES
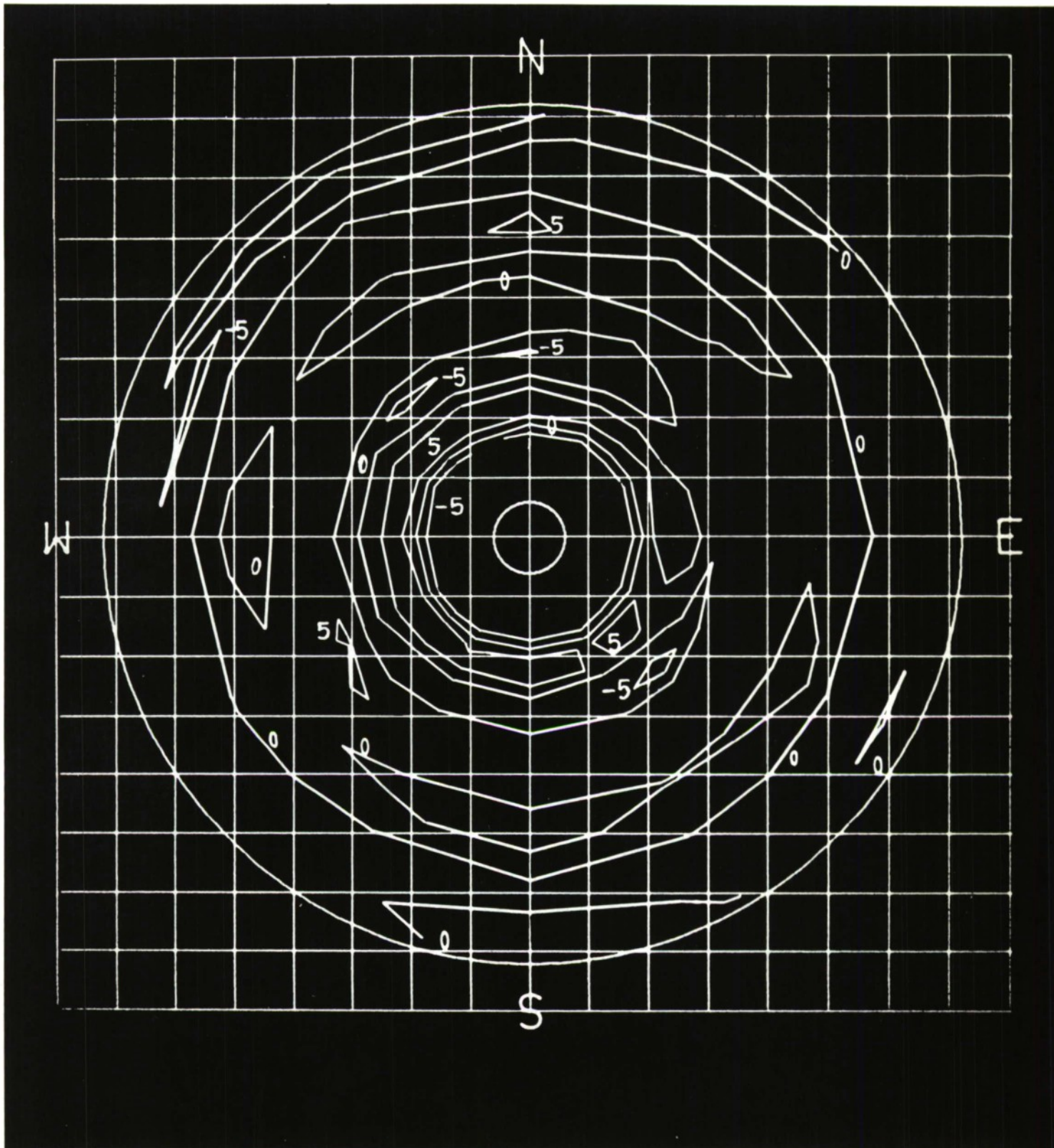
FIGURE 16 – CONTOUR MAP OF MEASURED EFFECTIVE SURFACE DEVIATIONS – DAYTIME SURVEY
CONTOUR INTERVAL = 50 MILS; ZENITH ANGLE = 0 DEGREES
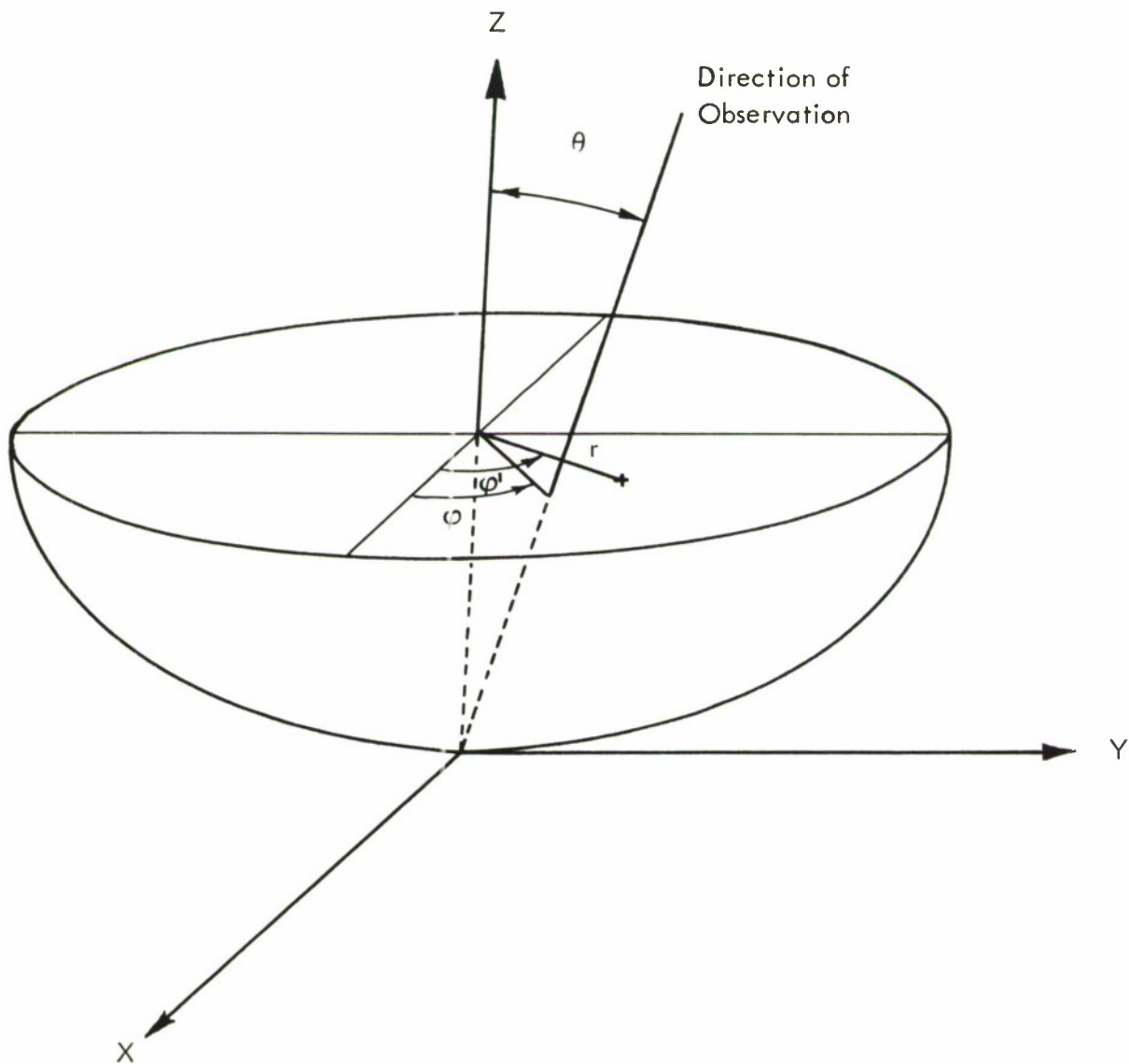
FIGURE 17 – COORDINATE SYSTEMS DEFINING DIRECTION OF
OBSERVATION AND APERTURE POSITION
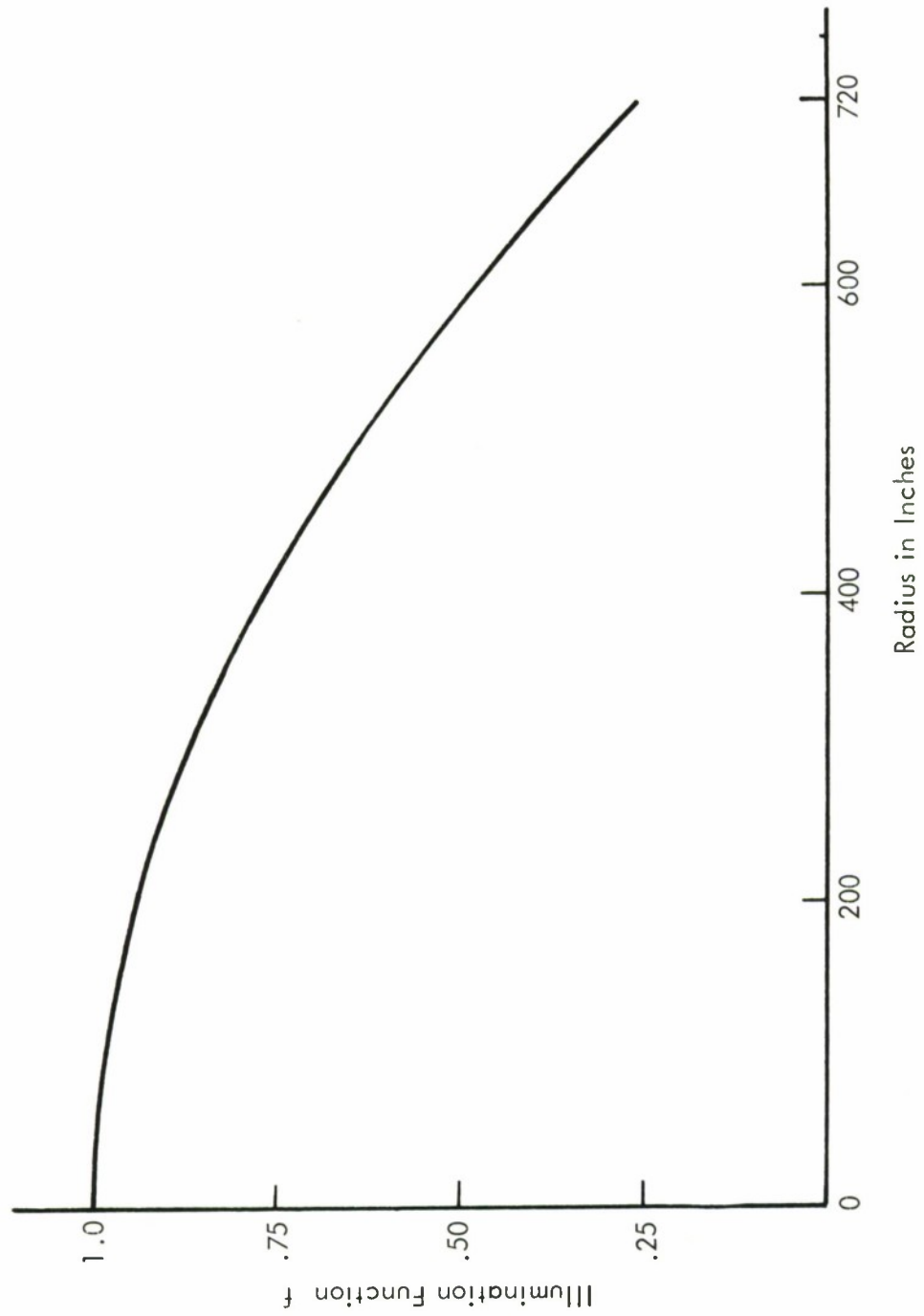
FIGURE 18 – VARIATION OF ASSUMED ILLUMINATION FUNCTION WITH RADIUS

78
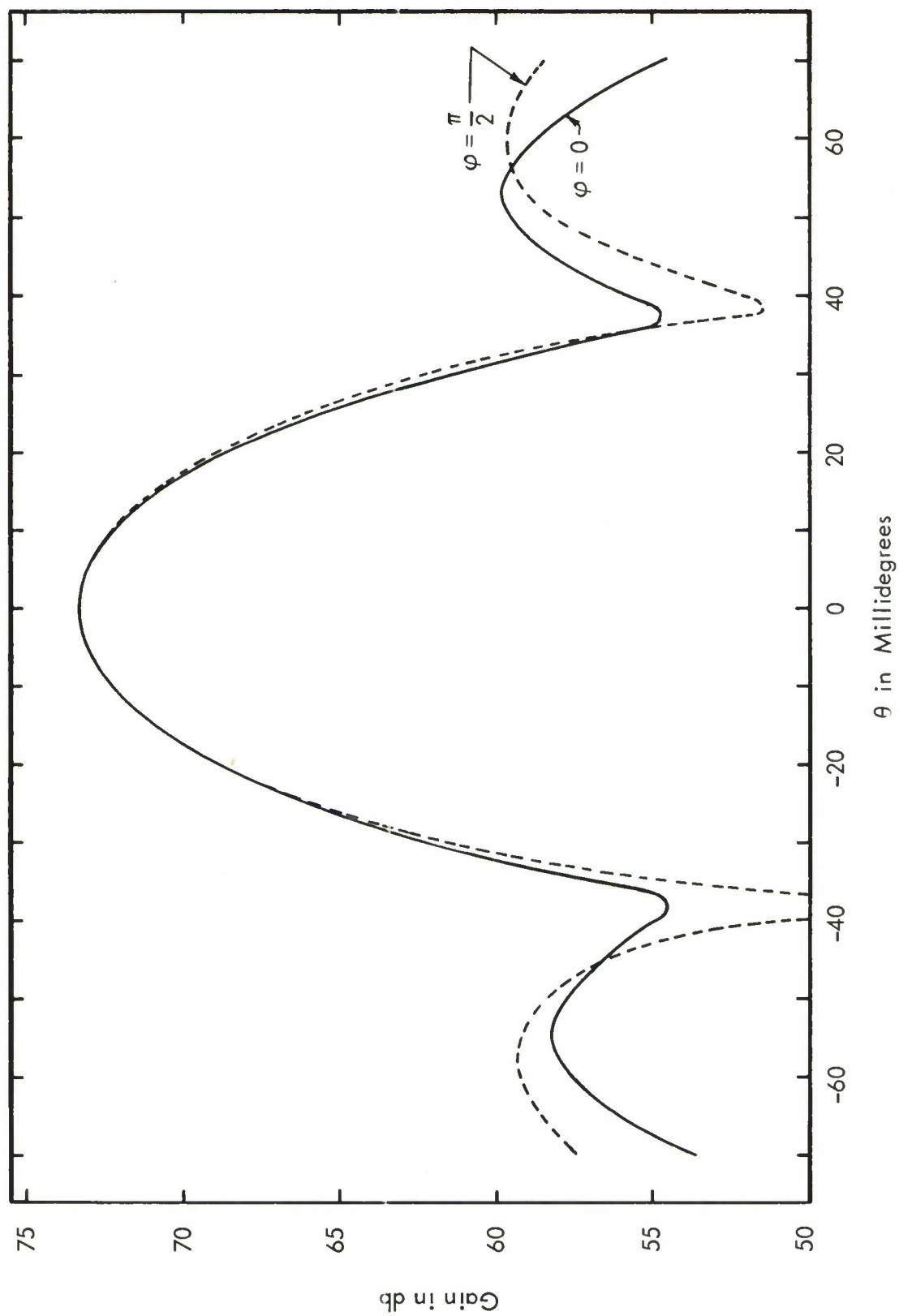
FIGURE 19 – RADIATION DIAGRAM FOR HAYSTACK ANTENNA AT 15.75 GHz CALCULATED FROM
NIGHT SURVEY; EDGE TAPER = 12 db

79
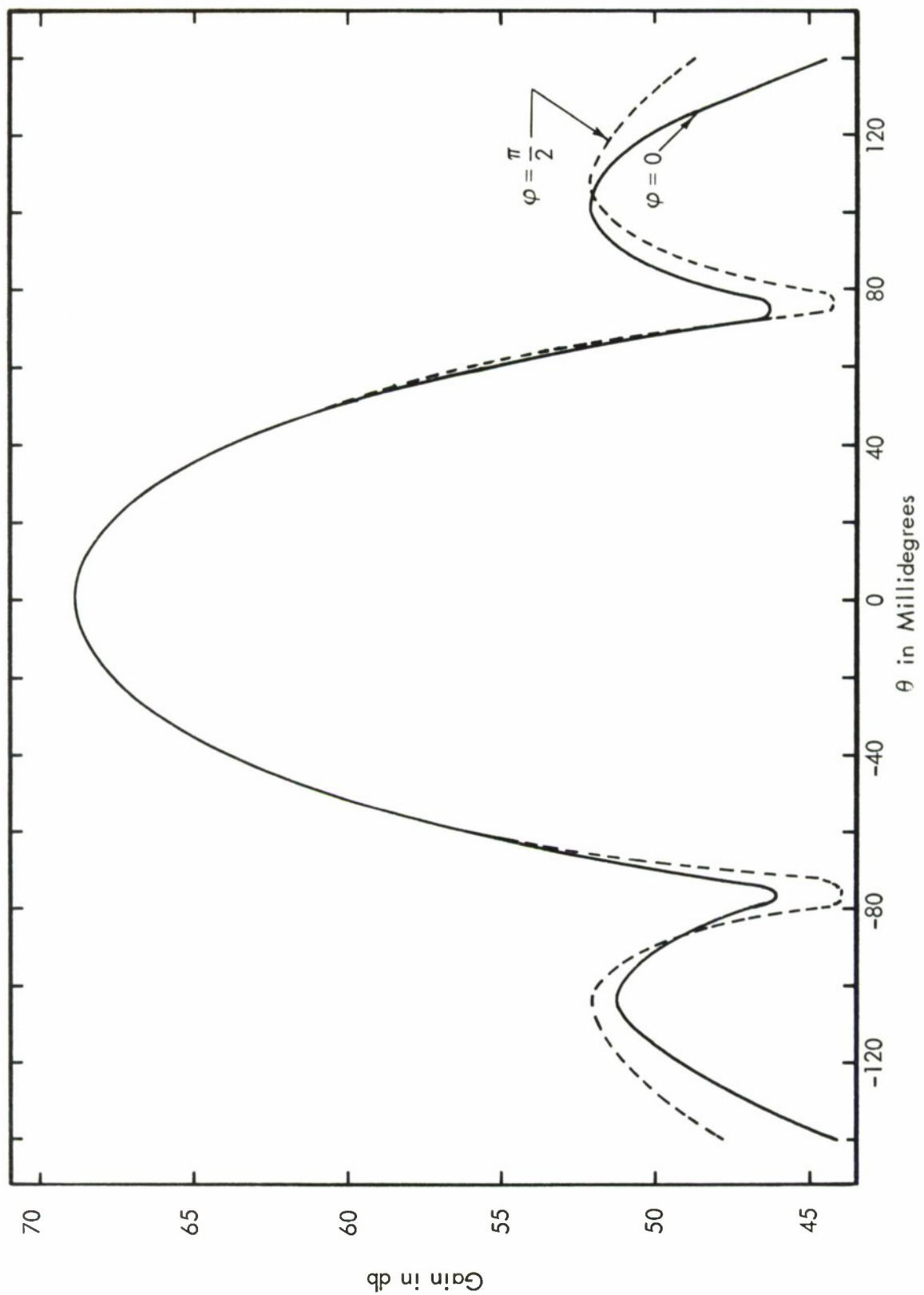
FIGURE 20 - RADIATION DIAGRAM FOR HAYSTACK ANTENNA AT 8.25 GHz CALCULATED FROM NIGHT SURVEY; EDGE TAPER = 12 db
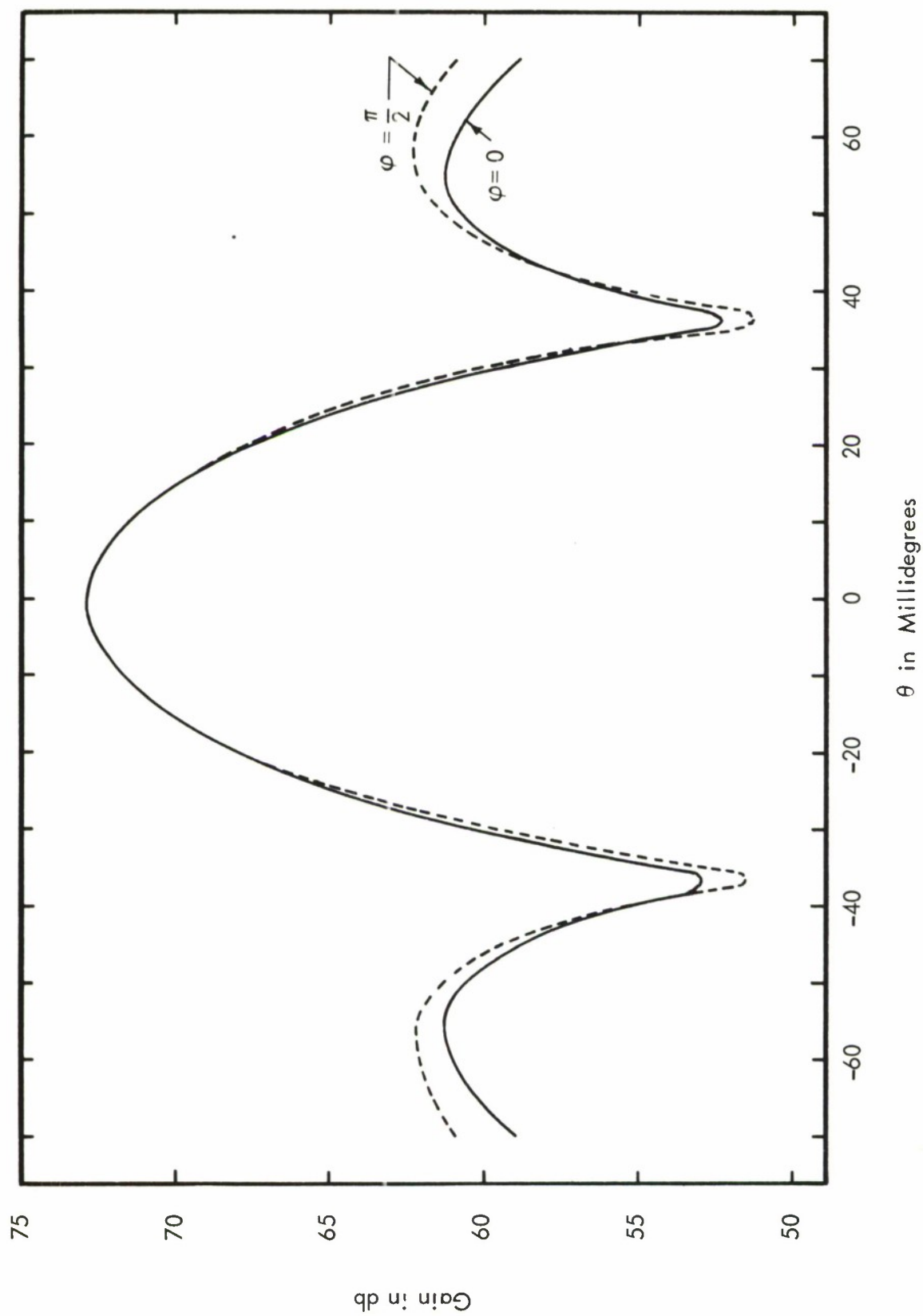
FIGURE 21 - RADIATION DIAGRAM FOR HAYSTACK ANTENNA AT 15.75 GHz CALCULATED FROM DAYTIME SURVEY; EDGE TAPER = 12 db
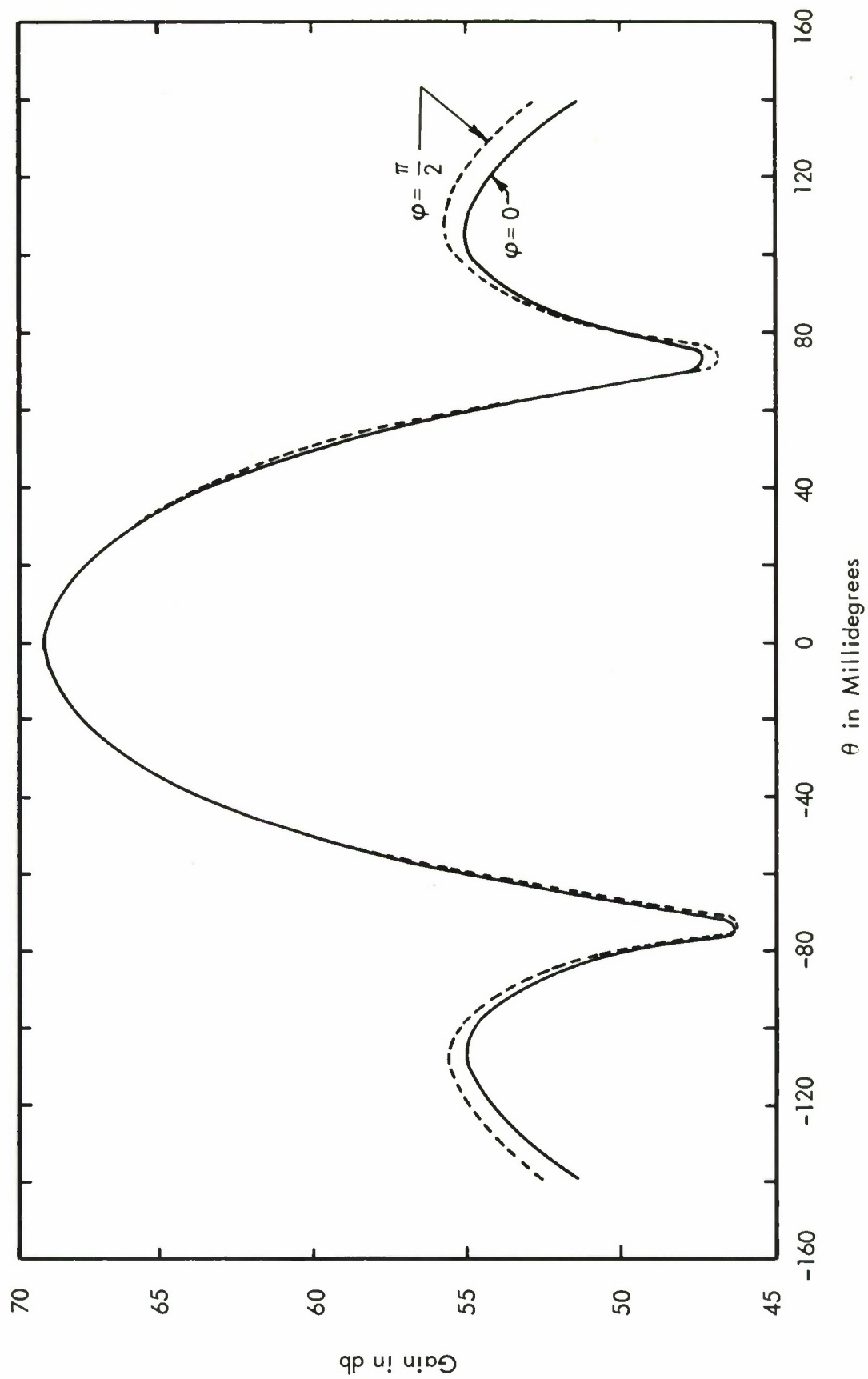
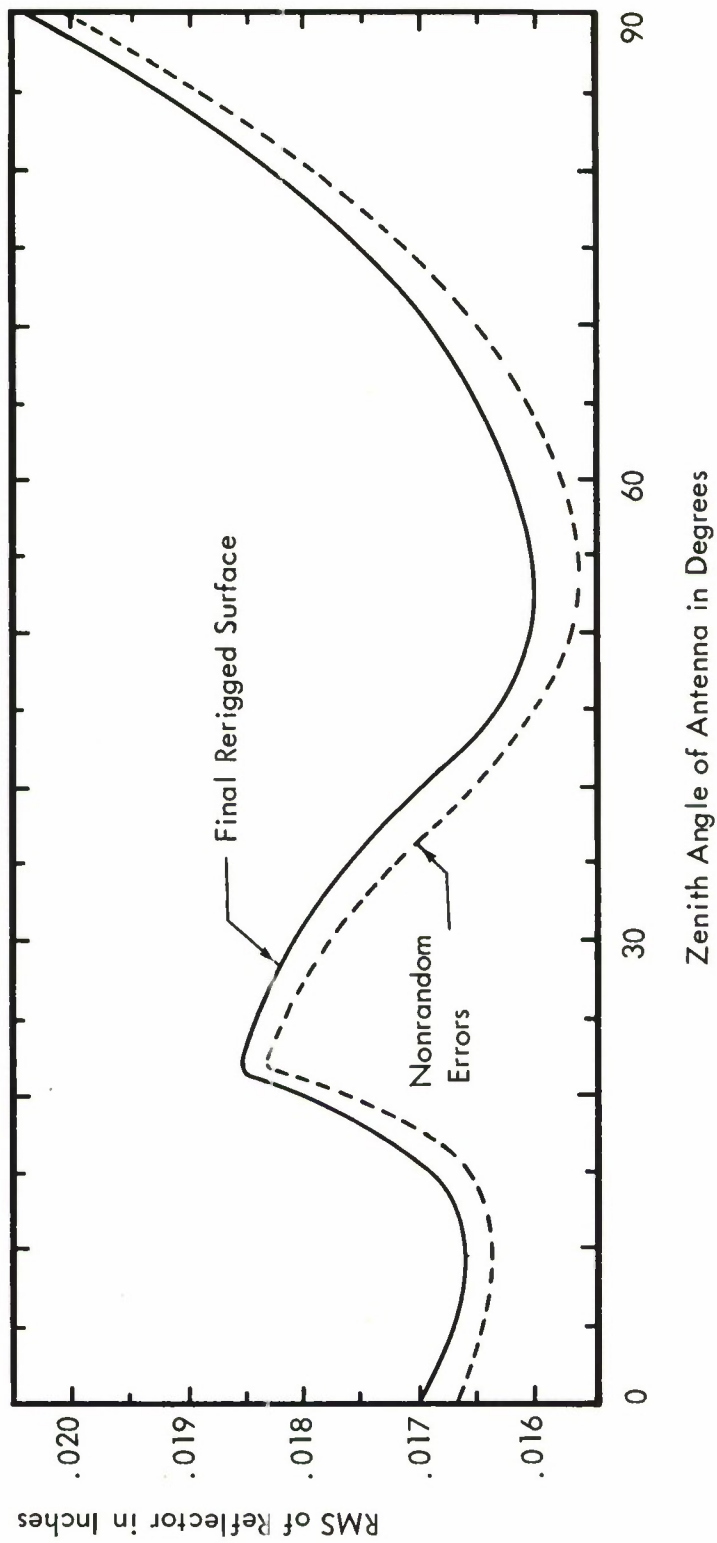FIGURE 22 - RADIATION DIAGRAM FOR HAYSTACK ANTENNA AT 8.25 GHz CALCULATED FROM DAYTIME SURVEY; EDGE TAPER = 12 db

82

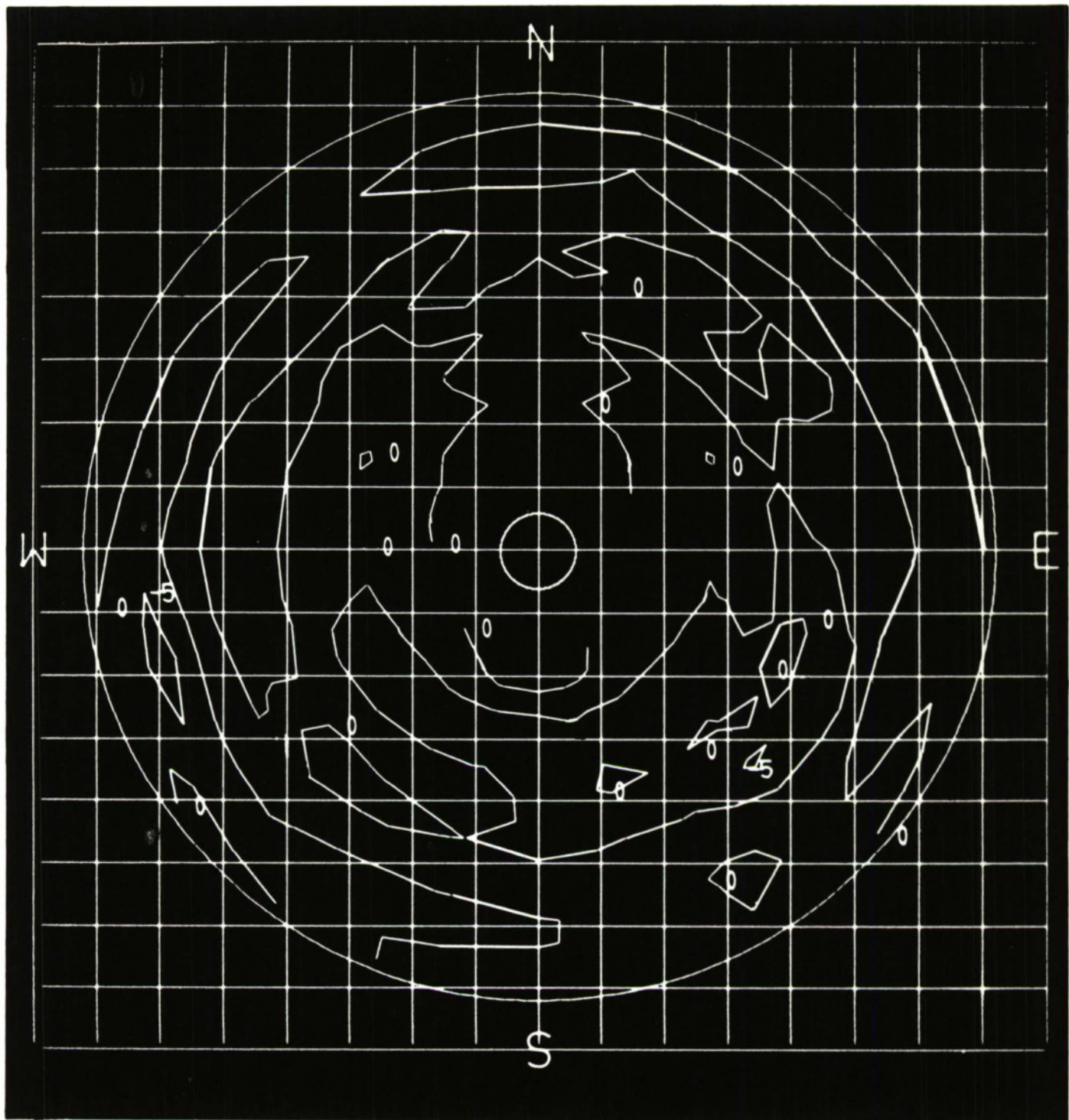FIGURE 23 – PREDICTED VARIATION OF RMS OF RERIGGED REFLECTOR WITH ZENITH ANGLE

83

FIGURE 24 – CONTOUR MAP OF PREDICTED EFFECTIVE SURFACE DEVIATIONS
OF RERIGGED ANTENNA
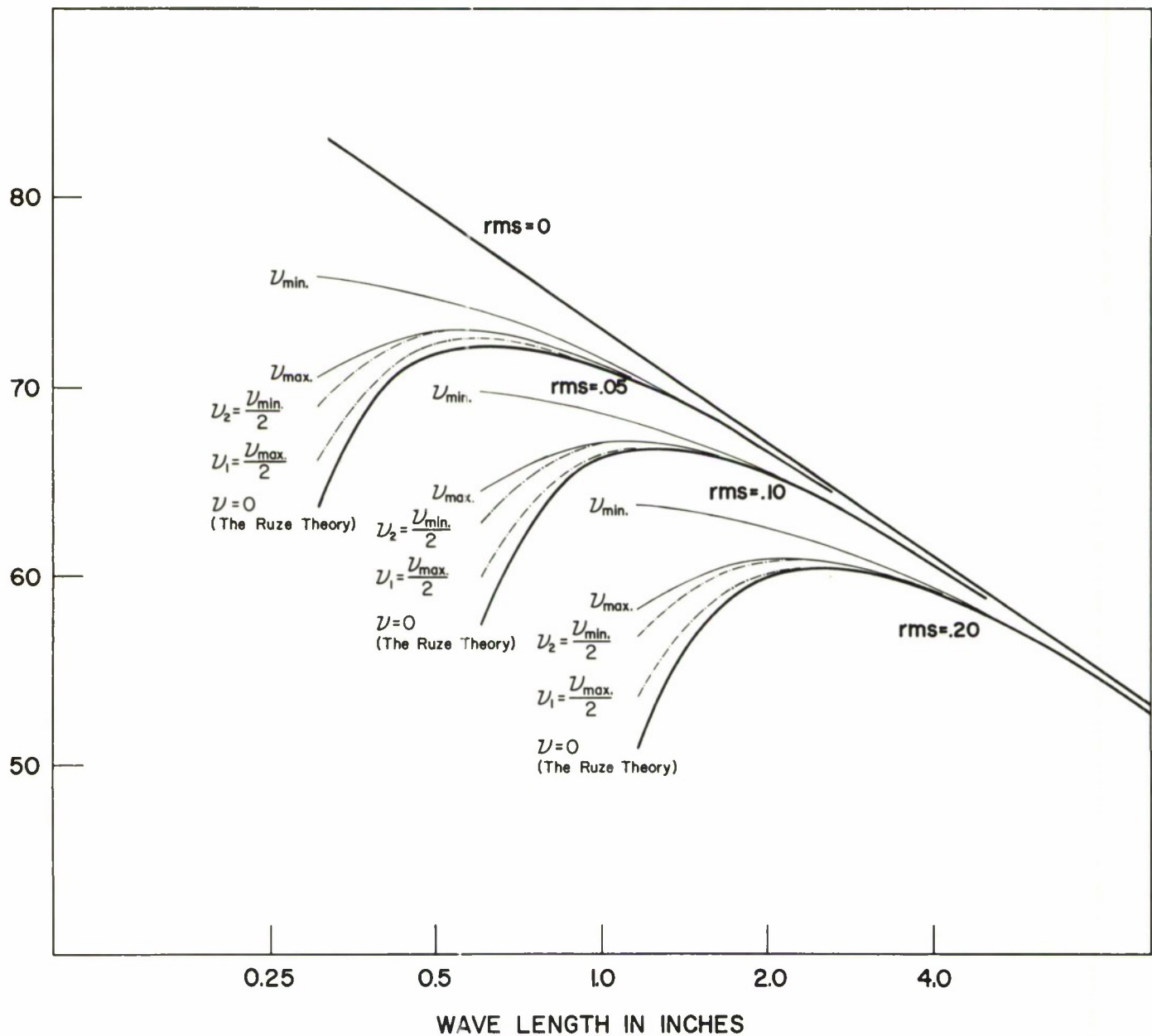
CONTOUR INTERVAL = 50 MILS; ZENITH ANGLE = 0 DEGREES

Figure 25-Variation of Gain of a Uniformly Illuminated 120-Foot Antenna with Wave Length for Different Magnitudes and Distributions of Surface Deviations.
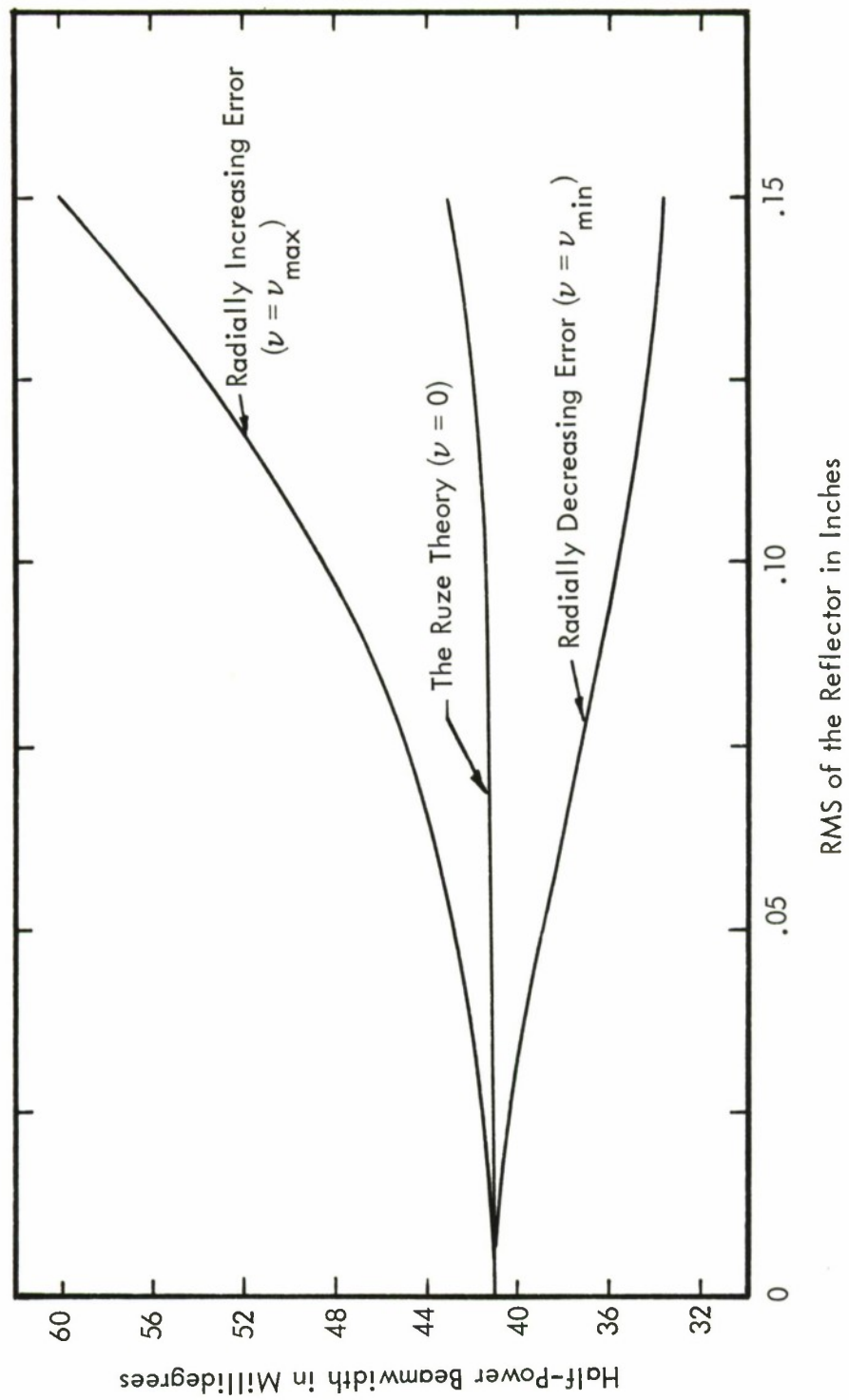
FIGURE 26 – VARIATION OF HPBW WITH THE RMS OF A 120-FOOT, UNIFORMLY ILLUMINATED REFLECTOR FOR VARIOUS DISTRIBUTIONS OF ERROR
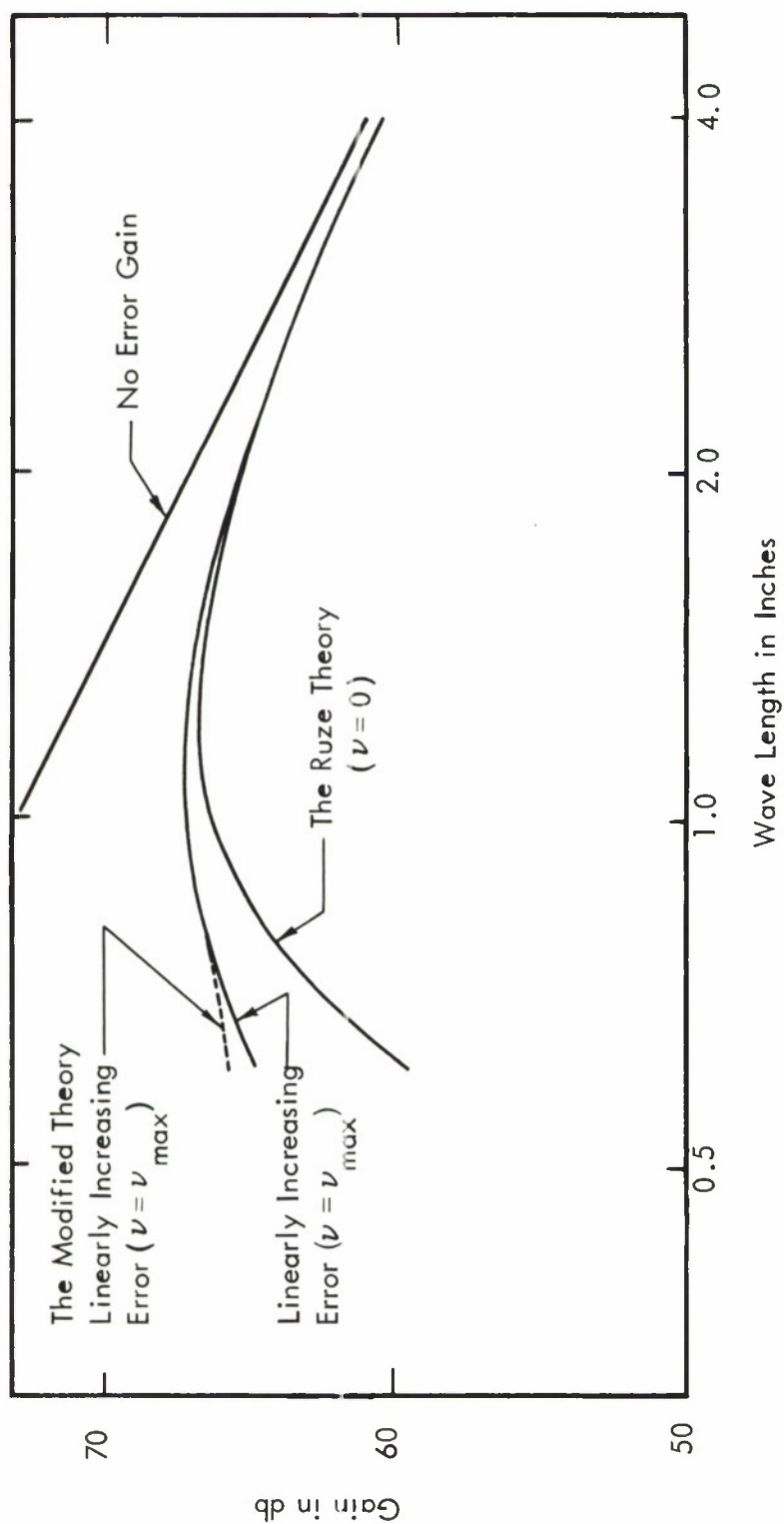
FIGURE 27 - COMPARISON OF MODIFIED THEORY WITH RUZE'S THEORY FOR LINEARLY INCREASING SURFACE DEVIATIONS OF A 120-FOOT REFLECTOR WITH UNIFORM ILLUMINATION, RMS = 0.1 INCHES
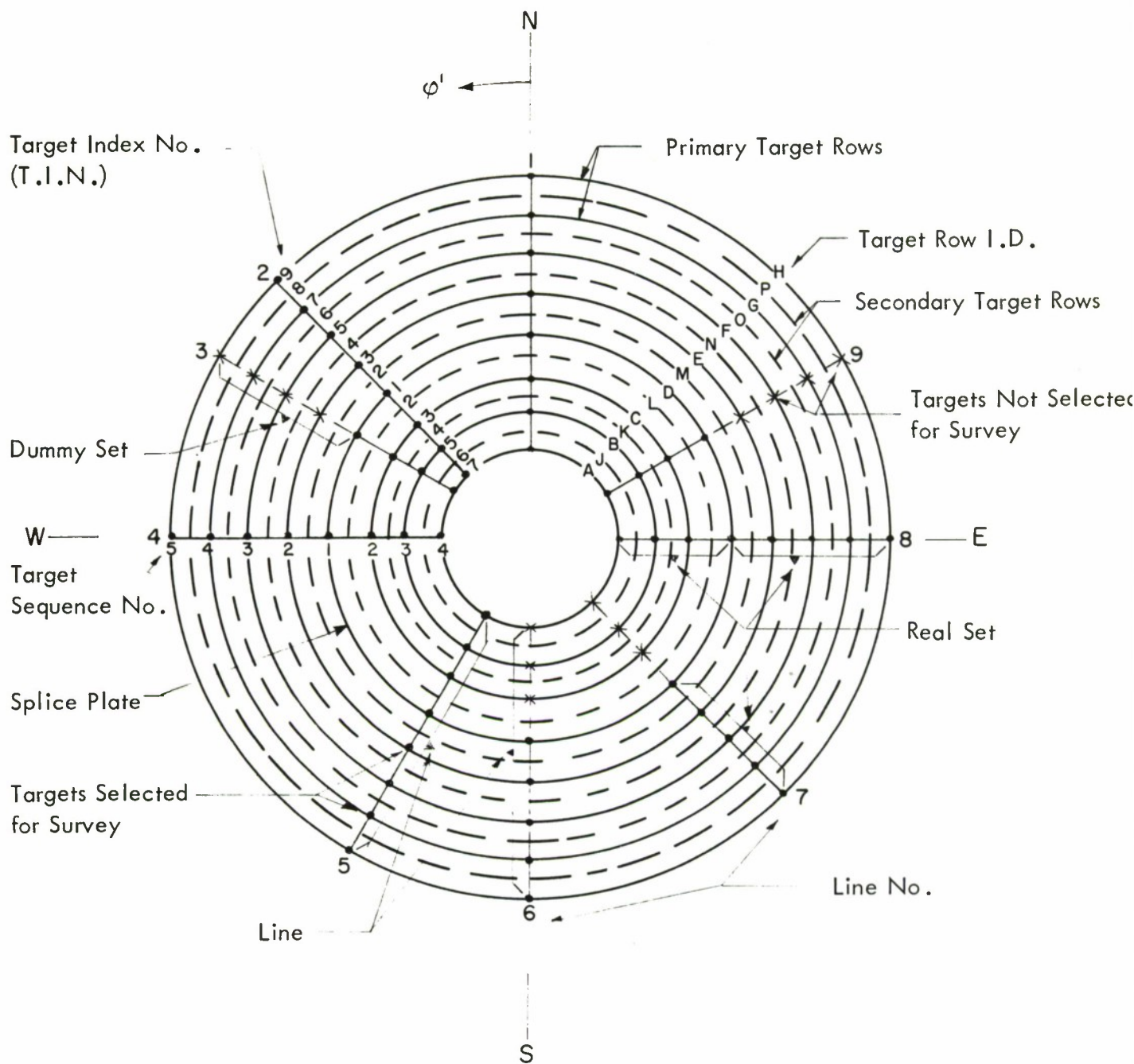
87

FIGURE 28 - TERMINOLOGY USED IN PROGRAM BESTFIT

DOCUMENT CONTROL DATA - R&D

(Security classification of title, body of abstract and indexing annotation must be entered when the overall report is classified)

1. ORIGINATING ACTIVITY *(Corporate author)* Simpson Gumpertz & Heger Inc. under Purchase Order No. C444 to Lincoln Laboratory, M. l. T.	2a. REPORT SECURITY CLASSIFICATION Unclassified
	2b. GROUP None

3. REPORT TITLE

Feasibility Study for Rerigging the Haystack Antenna

4. DESCRIPTIVE NOTES *(Type of report and inclusive dates)*

Final Report

5. AUTHOR(S) *(Last name, first name, initial)*

Simpson, Howard and Zarghamee, Mehdi S.

6. REPORT DATE 23 February 1967	7a. TOTAL NO. OF PAGES 100	7b. NO. OF REFS 15

8a. CONTRACT OR GRANT NO. AF 19(628)-5167	9a. ORIGINATOR'S REPORT NUMBER(S) SGH-668-1
b. PROJECT NO. 649L	
c.	9b. OTHER REPORT NO(S) *(Any other numbers that may be assigned this report)* ESD-TR-67-235
d.	

10. AVAILABILITY/LIMITATION NOTICES

Distribution of this document is unlimited.

11. SUPPLEMENTARY NOTES None	12. SPONSORING MILITARY ACTIVITY Air Force Systems Command, USAF

13. ABSTRACT

For the purpose of investigating the technical feasibility of rerigging the Haystack reflector, the following theoretical tools were developed:

1. A scheme was developed for the selection of an optimal sample of targets for predicting the error in the rms determination as affected by the size of sample.

2. Computer programs were written for processing and analysis of the optical surveys.

3. A statistical theory was derived for the prediction of surface deviations due to the random errors in the manufacture and rigging of the antenna.

4. A computer program was developed for the calculation of the radiation pattern of the reflector from the known surface errors.

5. An extension of Ruze's theory was developed for the prediction of the gain loss and scatter of reflectors with nonuniform error distributions.

The results of one night survey and one day survey were analyzed; the calculated rms was 37 mils and 41 mils, respectively. The larger surface errors occurred in the inner panel region.

The gain and the half-power beamwidths corresponding to the measured surface deviations were calculated; good correlation with radiometric measurements was obtained.

Based on a detailed analysis of the rerigged reflector, on the assumption that only the inner panels are rerigged, the rms under average thermal conditions is predicted not to exceed 25 mils. Some further improvement can be achieved if cable forces and their pick-up angles are optimized.

14. KEY WORDS

Haystack Hill	optical surveys
reflectors	radiometric measurements